Tellus (1983), *35B*, 206–236

The simultaneous use of tracers for ocean circulation studies

By BERT BOLIN, ANDERS BJÖRKSTRÖM and KIM HOLMÉN[1], *Department of Meteorology*[2], *University of Stockholm, Arrhenius Laboratory, S-106 91 Stockholm, Sweden* and BERRIEN MOORE, *University of New Hampshire, Complex Systems Research Center, O'Kane House, Durham, NH 03824, USA*

(Manuscript received September 2; in final form December 29, 1982)

ABSTRACT

A method for the simultaneous use of tracers for oceanic circulation studies is developed. To permit the inclusion of tracers that are subject to biochemical transformation a simple model for photosynthesis, bacterial decomposition and chemical dissolution is formulated based on the use of Redfield ratios for the chemical compounds interaction. The finite difference analogue to the steady state tracer continuity equation, applied to the tracers chosen, leads to a set of simultaneous algebraic equations that in principle can be solved by matrix inversion methods. Two cases are considered: (1) The problem is indeterminate, which may be the case when too few tracers are available and/or some tracer equations are redundant. A solution is obtained by minimizing the transport vector; (2) The problem is incompatible, which may result from making use of many tracers. A solution is obtained by minimizing the errors in satisfying the tracer continuity equations.

The method is applied to a 12-box model of the world oceans by considering the surface water, intermediate water, deep water and bottom water of the Arctic, Atlantic, Antarctic and Pacific/Indian Oceans (with some simplification for the polar seas). Total dissolved inorganic carbon, alkalinity, phosphorus, oxygen and radiocarbon are used as tracers. A series of steady state solutions are presented and the uncertainties as dependant on box configuration and erroneous or non-representative data are analysed.

In the reference solution, circulation cells emerge where Antarctic surface water penetrates into intermediate levels of the two major oceans, from where it undergoes lifting and, at the surface, advection back towards the south. In the Atlantic, much of the penetrating water reaches as far north as to involve the Arctic deep water, which sinks and moves towards the deep Antarctic Ocean through the deep Atlantic. The total upwelling in the Antarctic Ocean is about 30 Sv. Turbulent exchange prevails between surface and intermediate waters in both major oceans with an average K_z of about 1 $cm^2 s^{-1}$.

Particular consideration is given to the transfer of carbon by computing the changes in total carbon and radiocarbon that are induced by fossil fuel combustion and nuclear bomb testing by using the steady state circulation and turbulent transfer deduced. It is concluded that better spatial resolution is required to determine the role of the ocean as a sink for injections of carbon and radiocarbon.

1. The problem

The inhomogeneous distributions of chemical elements in the oceans have been used for many years to deduce features of the ocean circulation. For example, the tongue of low salinity water in the thermocline region extending northward from the Antarctic circumpolar convergence zone has been interpreted as northward flowing water, in which the relative magnitude of the advective flow to that of turbulent flux can be determined from the salinity profile. Similarly, the outflow of the

[1] Also at Department of Structural Chemistry, University of Stockholm, Arrhenius Laboratory, S-106 91 Stockholm, Sweden.

[2] Contribution No. 469.

Mediterranean water into the Atlantic Ocean can be followed by identification of a region of high salinity. In recent years the use of radioactive tracers, particularly those of ^{14}C and ^{3}H (tritium), has given important information on the water exchange between the surface layers, the intermediate waters and the deep sea (e.g. Munk, 1966; Kuo and Veronis, 1970; Keeling, 1973; Oeschger et al., 1975; Fine et al., 1981).

If the tracer is conservative (e.g. salt) or primarily affected by radioactive decay (e.g. ^{14}C, tritium) the problem is relatively simple, but most chemical tracers in the oceans are subject to biological and chemical transformations which are not quantitatively well understood. As a consequence, data have often been inadequate to find unique solutions, unless simplifying assumptions have been introduced. It is obviously important in such cases to use several tracers simultaneously to arrive at more conclusive results.

Using water continuity and six tracers (salinity, oxygen, dissolved inorganic carbon, ^{14}C of dissolved inorganic carbon, alkalinity and phosphorus), Keeling and Bolin (1967, 1968) studied the problem of the simultaneous use of a number of tracers for a three-box model of the world oceans (warm surface water, cold surface water and deep water). The processes of primary production of both organic matter and carbonate structure (shells) and their bacterial decomposition and chemical dissolution were included as internal source and sink terms for the chemical compounds considered. Also, exchanges of oxygen, inorganic carbon (as CO_2) and ^{14}C (as $^{14}CO_2$) between the atmosphere and the sea were described. It was found that the vertical turbulent exchange was primarily between the cold surface water and the deep sea, and the total flux of particulate inorganic and organic carbon were $1.0 \cdot 10^{15}$ and $1.7 \cdot 10^{15}$ g C yr^{-1}, respectively. This was in fair agreement with more direct but very approximate estimates. The turnover time for the deep water, determined by the ^{14}C difference between the surface water and the deep water, was 1100 years.

It is clear, however, that results obtained with such a crude representation of the ocean using only three reservoirs (boxes) in exchange with each other described by first order processes are to be considered as zero order estimates of the real processes that the model is intended to describe. The results are inadequate in that ordinary oceanographic data cannot be used for validation and we are still uncertain about how well such simple models give an answer to the question about the role of the oceans in the global carbon cycle. This is important since quantitatively accurate determination of the storage capacity of the oceans for carbon dioxide emitted into the atmosphere by burning fossil fuel and by changing land use are required in order to permit reliable projections of future CO_2 levels in the atmosphere as a result of future emission scenarios.

As will be shown in the present paper, it is possible to generalize the use of the equation for tracer continuity (diffusion equation), including simultaneously an advective term, to a number of tracers in a more detailed description of the ocean. In the present case we shall use dissolved inorganic carbon (DIC), alkalinity (A), phosphorus (P), oxygen (O) and ^{14}C. If we assume that turbulent processes can be described by an eddy diffusivity tensor, **K**, which is diagonal (components K_1, K_2 and K_3), then the water motions are described by a six scalar field defined by **K** and the advective velocity $\mathbf{V} = (V_1, V_2, V_3)$. Then proceeding as Keeling and Bolin (1968), but using better spatial resolution, we arrive at a large set of linear equations whose best fit solution can be obtained by using the pseudoinverse of the coefficient matrix.

Our general objective is to derive the most plausible spatial fields of **V** and **K** in the region concerned by making use of a number of stationary tracer distributions; moreover, the very fact that sets containing more than a thousand equations and unknowns can be solved with modern computors makes this technique appealing for interpretation generally of the increasing amount of data in the field of marine chemistry.

In the latter part of this paper we derive a simplified picture of the general circulation of the oceans based on this methodology. It is instructive in this first attempt to restrict the degrees of freedom in order to demonstrate some of the principal methodological problems that arise. In keeping with this view, the world oceans will be represented in this initial paper by merely 12 boxes, which of course implies considerable truncation errors both in the way the spatial distribution of the tracer data are used and in how the variables **K** and **V** are defined.

Comparison will be made with other estimates of

the character and intensity of the general circulation of the oceans as derived from direct measurement or dynamical determination and also with the much simpler 2-box or box-diffusion models as developed for analysis of the carbon dioxide problem (Keeling, 1973; Oeschger et al., 1975). We shall use the fields of **V** and **K** to simulate the transient behaviour of ^{14}C due to nuclear bomb testing as observed during the last 25 years and also determine the partitioning of CO_2 emitted by fossil fuel burning between the atmosphere and the oceans. It will become clear that even this better resolution is inadequate for a proper treatment of the CO_2 problem, but we shall learn how to proceed to establish more accurately the response characteristics of the oceans to a changing atmospheric CO_2 concentration.

While the present paper was being completed our attention was drawn to similar work by Wunsch and Minster (1982), in which case, however, the method of analysis was rather applied to the fields of temperature and salinity in the Northern Atlantic. It would of course be desirable to use simultaneously heat and salinity, as employed by Wunsch and Minster, and the chemical tracers as used in the present treatment. Also the fact that salinity and temperature determine the density field which in turn is related to the vertical change of the geostrophic flow could be used as an additional condition for the advective velocities that we wish to deduce. In this first analysis we shall, however, restrict our treatment merely to chemical tracers.

There was unexpected similarity in the mathematical approach in our analysis and that of Wunsch and Minster (1982). We shall, however, also treat the incompatible (overdetermined) problem and hope that the complementarity of the approach, as well as the differences, will shed additional light on this methodology. The results obtained in applying this method to the series of tracers mentioned before will also be of interest in the light of its possible extension to models with much better spatial resolution.

2. The continuity equation applied to a set of M tracers

2.1. *The finite difference form of the continuity equation*

We consider the tracer distributions q^m (x_1, x_2, x_3, t), where $m = 1, 2, \ldots M$ identifies the M tracers being considered. We denote by $\mathbf{V}$ (x_1, x_2, x_3, t) the advective water flux which is an average value over a space scale L and time scale T. Further we assume that the transfer of tracer material by eddies with space and time scales less than L and T respectively, can be described by eddy diffusion. Thus this transfer is given by $-\mathbf{K}\cdot\nabla q^m$, where $\mathbf{K}$ is the eddy diffusivity tensor. By proper choice of our coordinates x_1, and x_2 and x_3 we may assume that $\mathbf{K}$ is diagonal with the three components K_1, K_2 and K_3. Further, let Q^m (x_1, x_2, x_3, t) denote the sources (and sinks) for the tracer q^m and λ^m the radioactive decay constant. For any tracer q^m we then have

$$\frac{\partial q^m}{\partial t} = -\nabla\cdot(\mathbf{V}q^m) + \nabla\cdot(\mathbf{K}\cdot\nabla q^m) + Q^m - \lambda^m q^m \quad m = 1, 2, \ldots M \tag{2.1}$$

For a steady state we have $\partial q^m/\partial t = 0$. As boundary conditions we need to specify the net flux in or out of the water body that is being considered, i.e. the exchange with the atmosphere, the sediments or parts of the ocean which are not explicitly treated.

We shall also assume that water continuity is given by

$$\nabla\cdot\mathbf{V} = 0 \tag{2.2}$$

and prescribe a zero flux boundary condition for the exchange of water across external boundaries.

The M equations (2.1) will be applied simultaneously to known distributions of q^m to determine $\mathbf{V}$ and $\mathbf{K}$. To arrive at a finite difference formulation we divide the water body under consideration into a number of boxes $i = 1, 2, \ldots I$, the boundaries of which are parallel with the axes of the coordinate system (cf. Keeling and Bolin, 1967, 1968). By integration of (2.1) and (2.2) over any such box we get

$$\int_{A_i}\left(v_n q^m - K_n\frac{\partial q^m}{\partial x_n} - f_e^m\right)\mathrm{d}A = \int_{W_i}(Q^m - \lambda^m q^m)\,\mathrm{d}W \tag{2.3}$$

where index i refers to the box being considered and n takes on the values 1, 2, 3 when the boundary surface is perpendicular to the axes x_1, x_2 and x_3 respectively; $\mathrm{d}A$ is a surface element and $\mathrm{d}W$ is a volume element. The term f_e^m, the flux

across an external boundary, appears whenever the box i is at the boundary of the domain.

For any boundary surface A_{ij} between box i and adjacent box j we write

$$\int_{A_{ij}} \left(v_n q^m - K_n \frac{\partial q^m}{\partial x_n} \right) \mathrm{d}A = v_{ij} \int_{A_{ij}} q^m \mathrm{d}A - K_{ij} \int \frac{\partial q^m}{\partial x_n} \mathrm{d}A \tag{2.4}$$

where x_n is perpendicular to the surface A_{ij}. In this way v_{ij} and K_{ij} are the mean advective water flux and turbulent exchange coefficient across the boundary surface between boxes i and j. Further, define $\hat{Q}_i$, $\hat{q}_i^m$, N_i^m and F_{ei}^m by

$$\begin{cases} \hat{Q}_i^m W_i = \int_{W_i} Q_i^m \mathrm{d}W \\ N_i^m = \hat{q}_i^m W_i = \int_{W_i} q_i^m \mathrm{d}W \\ F_{ei}^m = \int_{A_{ei}} f_e^m \mathrm{d}A \end{cases} \tag{2.5}$$

Thus F_{ei}^m is the flux of tracer m to or from box i at the external boundary.

If $\hat{Q}_i^m$ depends on biological processes, i.e. primary production and decomposition of detritus, we may use Redfield's (1958) approach to interrelate these. Let F_{oi} denote the net primary production (or decomposition) of organic matter and F_{ci} correspondingly be the formation (or dissolution) of carbonates. Further, γ_o^m and γ_c^m are the Redfield ratios between element m and carbon involved in these processes. We then have

$$\hat{Q}_i^m W_i = \gamma_o^m F_{oi} + \gamma_c^m F_{ci} \tag{2.6}$$

Eq. (2.3) may then be transformed into

$$\sum_j v_{ij} \int_{A_{ij}} q^m \mathrm{d}A - \sum_j K_{ij} \int_{A_{ij}} \frac{\partial q^m}{\partial x_n} \mathrm{d}A - \gamma_o^m F_{oi} - \gamma_c^m F_{ci} = -\lambda^m N_i^m + F_{ei}^m \qquad i = 1, 2, \ldots I \quad m = 1, 2, \ldots M \tag{2.7}$$

where the summations are extended over the values j that refer to adjacent boxes. F_{oi} and F_{ci} will also be considered as unknowns, to be determined.

We similarly derive the finite difference approximation of the water continuity equation (2.2)

$$\sum_j v_{ij} = 0 \qquad i = 1, 2, \ldots I \tag{2.8}$$

Eqs. (2.7) and (2.8) constitute a set of $(M + 1) \cdot I$ simultaneous equations for the $2L + 2I$ unknowns v_{ij}, K_{ij}, F_{oi} and F_{ci} where L denotes the total number of surfaces between adjacent boxes. The coefficients of v_{ij}, K_{ij}, F_{oi} and F_{ci} depend on data and known values for γ_o^m and γ_c^m and constitute a matrix, which will be denoted by $\mathbf{A} \cdot [a_{rs}]$. The unknown variables v_{ij}, K_{ij}, F_{oi} and F_{ci} may be considered as a vector, $\mathbf{x}$, which has the dimension $2(L + I)$ and similarly the inhomogeneous terms $(-\lambda^m N_i^m + F_{ei}^m)$ constitute another vector to be denoted by $\mathbf{b}$. The set of eqs. (2.7) and (2.8) can then be written

$$\mathbf{A}\mathbf{x} = \mathbf{b} \tag{2.9}$$

With given data on the tracer distributions q_i^m we can determine $\mathbf{A}$ and $\mathbf{b}$ and in principle we can solve for $\mathbf{x}$. Rather than evaluating the coefficients of $\mathbf{A}$ as the integrals given in (2.5) and (2.7) we shall assume that q_i^m is the value of q^m in the centre of the box and put

$$\begin{cases} \int_{A_{ij}} q^m \mathrm{d}A = \tfrac{1}{2}(q_i^m + q_j^m) A_{ij} \\ \int_{A_{ij}} \frac{\partial q^m}{\partial x_n} \mathrm{d}A = (q_i^m - q_j^m) \frac{A_{ij}}{\Delta_{ij}} \end{cases} \tag{2.10}$$

where Δ_{ij} is the distance between the centre points of adjacent boxes. The vector $\mathbf{x}$ will then be defined to have the components

$$\mathbf{x} = \mathbf{x}\left(v_{ij} \cdot A_{ij}, \frac{K_{ij}}{\Delta_{ij}} A_{ij}, F_{oi}, F_{ci} \right) \tag{2.11}$$

We note that $v_{ij} A_{ij}$ and $K_{ij} \cdot A_{ij} / \Delta_{ij}$ are in the same units ($\mathrm{m^3\ yr^{-1}}$) and that the latter expresses the turbulent water flux across the interface. The fact that $v_{ij} \cdot A_{ij}$, $K_{ij} A_{ij} / \Delta_{ij}$ on one hand and F_{oi}, F_{ci} on the other do not have the same dimensions must be taken into account in deriving a solution (see further, Section 2.3).

In addition to the set of tracer equations that defines the matrix $\mathbf{A}$ we may include other relations between the variables defined as components of the vector $\mathbf{x}$ in order to put further constraints on our solution. In the present case we shall assume that the net formation of detritus in the surface boxes is balanced by decomposition and dissolution in the boxes underneath, i.e. no significant deposition takes place at the bottom. Formally we write

$$\begin{aligned} (F_{oi})_{\text{surface}} &= \sum_i F_{oi} \\ (F_{ci})_{\text{surface}} &= \sum_i F_{ci} \end{aligned} \tag{2.12}$$

where the summations are extended over the appropriate boxes below each surface box under consideration. If S denotes the number of surface boxes, $2S$ additional equations are obtained. Henceforth the set of equations (2.9) is assumed to include those specified by (2.12).

2.2. *Criteria for the choice of a unique solution*

The matrix $\mathbf{A} = [a_{rs}]$ in eq. (2.9) has the dimension $r \times s$ where $r = I(M + 1) + 2S$ and $s = 2(L + I)$. An equation system of this kind is often said to be underdetermined if $r < s$ and overdetermined if $r > s$. However, since some rows may be linear combinations of other rows (and indeed this is the case in the present investigation) the rank, not the dimension of $\mathbf{A}$, is important. Even when $r < s$ a system may be overdetermined in the sense that no set of numbers will satisfy all equations simultaneously. Similarly, when $r > s$ the system can still be underdetermined in the sense that more than one solution may exist. A different terminology will therefore be useful.

A system of linear equations with more than one exact solution will be said to be *indeterminate*. If a system has no exact solutions, we refer to it as *incompatible* (Shilov, 1961). We recall from linear algebra that

(i) if $r < s$, any compatible system is indeterminate. However, to a given matrix $\mathbf{A}$ there may exist vectors $\mathbf{b}$ such that (2.9) is incompatible;

(ii) if $r > s$, then to any matrix $\mathbf{A}$ there exist vectors $\mathbf{b}$ such that (2.9) is incompatible. If $\mathbf{b}$ is approximated by a vector $\mathbf{b}_p$ for which solutions exist, the system $\mathbf{Ax} = \mathbf{b}_p$ may or may not be indeterminate.

In cases of compatible systems, there still may not exist a "realistic" solution even though more than one "mathematical" solution exists. If there are realistic solutions, one must have a logically comparable methodology to select one "preferred" solution among them. We will require that the solution vector $\mathbf{x}$ be of smallest length. This choice to minimize the norm of $\mathbf{x}$ may well be questioned. There is no physical reason why the ocean, given a certain distribution of chemical elements, should preferably have the "slowest" circulation pattern that can be reconciled with these distributions. This solution is of some interest since it probably would yield a small capacity for uptake of atmospheric CO_2. This is clearly of interest when subjecting the solution to time integration.

In order to study the case where no solution, physically realistic or not, exists, one must relax the condition $\mathbf{Ax} = \mathbf{b}$ and simply attempt to minimize the norm $\|\mathbf{Ax} - \mathbf{b}\|$ where $\| \ldots \|$ is taken to mean the euclidean norm and $\mathbf{x}$ is allowed to vary over the set of all realistic vectors. In fact, this implies that no equations are identically satisfied and this also applies for the equations of water continuity. This is of importance, when we wish to use $\mathbf{x}$ in computing changes of the tracer distributions as a consequence of external sources and sinks (fossil fuel carbon emissions and bomb ^{14}C emissions to the atmosphere), see further, Section 6. This could, however, be avoided by defining the advective velocities in terms of a stream function.

In each case, the concept of a "realistic solution" must be given a mathematical formulation. In physical terms, the conditions we pose on a realistic solution are (a) that the turbulent fluxes do not occur against the tracer gradients and (b) that production of biogenic material must occur in the surface layer, with decomposition in the boxes below. Recalling the composition of $\mathbf{x}$ (2.11) we can formulate these conditions

$$\left.\begin{matrix} x_i \geq 0 \\ x_i \leq 0 \end{matrix}\right\} \text{for appropriate values of } i. \tag{2.13}$$

Searching for suitable algorithms, we found that the available library programs allow for the more complex set of constraints

$$\sum_{j=1}^{s} g_{ij}\, \chi_j \geq h_i \quad \text{for all } i = 1, 2, \ldots r \tag{2.14}$$

or, in shorter notation, $\mathbf{Gx} \geq \mathbf{h}$ (where $\mathbf{G} = [g_{ij}]$). It is easily realized that the conditions (2.13) can be written in the form (2.14) by setting $g_{ij} = -1$, 0 or 1 and $h_i = 0$ for appropriate values of i and j.

In the following, we therefore treat the *incompatible* case by solving a problem that can be formulated (Method I):

> Given $r \times s$ matrix $\mathbf{A}$ (with $\mathbf{A}$ having full column rank), $q \times s$ matrix $\mathbf{G}$, r-dimensional vector $\mathbf{b}$, and q-dimensional vector $\mathbf{h}$, find an s-dimensional vector $\mathbf{x}$ such that $\|\mathbf{Ax} - \mathbf{b}\|$ is minimum and $\mathbf{Gx} \geq \mathbf{h}$.

For the *indeterminate* case we solve a problem

that can be formulated (Method II):

Given $r \times s$ matrix **A**, $q \times s$ matrix **G**, r-dimensional vector **b**, and q-dimensional vector **h** find an s-dimensional vector **x** such that $\mathbf{Ax} = \mathbf{b}$, $\mathbf{Gx} \geq \mathbf{h}$ and $\|\mathbf{x}\|$ is minimal.

Because of the choice of norm that we have made these are "least square" problems. They will cover all systems addressed in the present paper. Method II is always applicable when *exact* and realistic solutions to (2.9) exist; as for Method I we must require that the rank of **A** equals the number of columns. Some mathematical details are presented in an appendix. The work of Lawson and Hanson (1974, Chapter 23) is particularly germane.

We regret that we have not found a logically comparable methodology that applies to all systems. This subject will be explored further in subsequent papers.

2.3. *Scaling*

The components of **x**, i.e. $v_{ij}A_{ij}$, $K_{ij}\cdot A_{ij}/\Delta_{ij}$, F_{oi}, F_{ci} have different dimensions and so have the different equations of the system $\mathbf{Ax} = \mathbf{b}$. In minimizing $\|\mathbf{x}\|$, the indeterminate case, or $\|\mathbf{Ax} - \mathbf{b}\|$, the incompatible case, proper scaling must be introduced.

(i) *Minimizing* $\|\mathbf{x}\|$. $v_{ij}\cdot A_{ij}$ and $K_{ij}\cdot A_{ij}/\Delta_{ij}$ have the dimension of volume of water per unit time, while F_{oi} and F_{ci} have the dimensions of mass of carbon per unit time. Since we are primarily concerned with the transfer of carbon it seems reasonable to multiply $v_{ij}\cdot A_{ij}$ and $K_{ij}\cdot A_{ij}/\Delta_{ij}$ by the average concentration of carbon in the sea, even though other choices are conceivable.

(ii) *Minimizing* $\|\mathbf{Ax} - \mathbf{b}\|$. In this case we search for the vector **x** that minimizes the errors when satisfying the r equations of our system. There are several circumstances to consider. The choice to be made will be given in Section 4.3.

(a) The accuracy with which the tracer distributions are known varies. Both the accuracy of individual observations and their representativeness matter in this context. We may for this reason ask for different accuracies in satisfying the tracer continuity equation for different compounds.

(b) The chemical interactions of the different tracers take place through the terms F_{oi} and F_{ci} and are determined by the Redfield ratios γ^m. Equivalency with regard to their contributions in computing the norm $\|\mathbf{Ax} - \mathbf{b}\|$, the equations of continuity for C, A, P and O should be multiplied by $(\gamma^m)^{-1}$, m = C, A, P, O respectively (see further, Section 3.2).

(c) The ^{14}C equations are the only ones that provide an absolute time scale because of radioactive decay. If we consider this *absolute* scale more important than the *relative* role of different parts of the ocean circulation, the ^{14}C equations should be given more weight.

(d) Phosphorus and oxygen interact through F_{oi} in a reciprocal way. In order not to give undue weight to the processes of photosynthesis of organic tissue and bacterial decomposition by making use of both tracers, they might be scaled down.

3. Specification of physical, chemical and biological processes

Being concerned with the carbonate system of the sea and in view of the role of primary production in determining the distribution of the carbon compounds in the sea, we shall consider the following elements

m = C, dissolved inorganic carbon, DIC
= *, dissolved inorganic ^{14}C
= A, total alkalinity
= P, phosphorus
= O, oxygen

3.1 *Air–sea exchange*

We need to consider air–sea exchange for the three tracers C, ^{14}C and O. The exchange coefficient for CO_2 across the air–sea interface is determined so that the flux of ^{14}C into the sea is equal to the decay within the sea. Without significant loss of accuracy fractionation can be omitted in the treatment of the C exchange. It must not be disregarded, however, when concerned with the transient transfer of CO_2 and ^{14}C (see further, Section 6). We define

$$R_{io} = \frac{N^*_{io}/N^C_{io}}{N^*_{ao}/N^C_{ao}} \tag{3.1}$$

where N^C_i denotes the total amount of carbon in box i, subscript a refers to the atmosphere and o to steady state conditions. R_{io} has been adjusted to the

$^{13}C/^{12}C$ ratio postulated for average terrestrial wood to account for fractionation. We further denote by e the air–sea exchange flux and deduce on the basis of the assumption of balance between net flux of ^{14}C into the surface waters and radioactive decay.

$$e = \frac{\lambda \sum_{l=1}^{I} R_{lo} N_{lo}}{\sum_{l} A_{la} \varepsilon_{la} - \sum R_{lo} A_{la} \varepsilon_{la}} \tag{3.2}$$

where the summations in the denominator are over all surface boxes, which have a surface area A_{la}. An enhancement factor ε_{la} has been introduced to account for areal variations of air–sea exchange rate. It is assumed that $\sum_l \varepsilon_{la} A_{le} = \sum_l A_{le}$. We will consider the effects of the latitudinal dependence of the exchange rate (cf. Peng et al., 1979) and the influence of the presence of sea ice. We further define the turn-over time of CO_2 in the atmosphere with respect to atmosphere–ocean exchange.

$$\tau_a = \frac{N_a}{e \sum_i \varepsilon_{ia} A_{ia}} \tag{3.3}$$

where the summation is over all surface boxes. The fluxes of carbon across the air–sea interface are subsequently calculated by

$$\begin{cases} F_{ai}^{C} = p_a \dfrac{e}{p_{ao}} A_{ia} \\ F_{ia}^{C} = p_i \dfrac{e}{p_{ao}} A_{ia} \end{cases} \tag{3.4}$$

where p_a and p_i are the partial pressures of CO_2 in the air and in the surface water reservoir and P_{ao} is the partial pressure of CO_2 at steady state. The fluxes of ^{14}C are given by

$$\begin{cases} F_{ai}^{*} = F_{ai}^{C} \dfrac{N_a^{*}}{N_a} \\ F_{ia}^{*} = F_{ia}^{C} \dfrac{N_i^{*}}{N_i} \end{cases} \tag{3.5}$$

p_i is calculated from the DIC and alkalinity values of each surface box. The data used must not be salinity normalized. Applied to any surface box we have (omitting for convenience the subscript i):

$$[H^+] + q^A = \frac{k_w}{[H^+]} + \frac{k_B \cdot q^B}{[H^+] + k_B} + \\ + \frac{[H^+]k_1 + 2k_1k_2}{[H^+]^2 + [H^+]k_1 + k_1k_2} \cdot q^C. \tag{3.6}$$

p is given by

$$p = \frac{[H^+]^2}{[H^+]^2 + [H^+]k_1 + k_1k_2} \cdot \frac{q^C}{k_0}. \tag{3.7}$$

The equilibrium constant for the first (k_1) and second (k_2) dissociations of CO_2 are taken from Mehrbach et al. (1973) and the dissociation constant for $B(OH)_3$, (k_B) and the dependence of the borate concentration (q^B) on salinity are from Almgren et al. (1975). The dissociation constant for water (k_w) is obtained from the tables of Hanson (1973). The solubility of CO_2 (k_0) as reported by Weiss (1974) is used.

The air–sea exchange of oxygen is modelled in a simpler fashion. An instantaneous equilibrium is assumed in all surface boxes, since the time for equilibrium is short (Broecker and Peng, 1974). The solubility of oxygen as determined by Weiss (1970) is used in the calculations.

3.2. *Detritus fluxes*

We distinguish between organic and inorganic detritus fluxes of carbon. The inorganic detritus is pure calcium carbonate.

The organic material is generalized as $(CH_2O)_{\gamma^C}(NH_3)_{\gamma^N} \cdot (H_3PO_4)_{\gamma^P}$ where γ^C, γ^N and γ^P are the "Redfield" ratios (1, 16/106, 1/106; cf. Redfield, 1958).

$$(CH_2O)_{\gamma^C} \cdot (NH_3)_{\gamma^N} \cdot (H_3PO_4)_{\gamma^P} + (\gamma^C + 2\gamma^N)O_2 + \\ + (\gamma^C + \gamma^N + 2\gamma^P)CO_3^{2-} \underset{\text{assimilation}}{\overset{\text{oxidation}}{\rightleftharpoons}} \gamma^N NO_3^- + \\ + (2\gamma^C + \gamma^N + 2\gamma^P)HCO_3^- + \gamma^N H_2O. \tag{3.8}$$

Thus the fluxes of organic material transport $(-\gamma^N - \gamma^P)$ equivalents of alkalinity for every γ^P moles of carbon. The oxidation states of nitrogen and phosphorus in the organic material are uncertain, creating uncertainties in oxygen consumption; however, the dominating oxidation process is, of course, the oxidation of carbon. We may put $\gamma^O = -(\gamma^C + 2\gamma^N)$. No preferential dissolution processes have been considered (e.g. the release of

phosphorus in shallower layers, whilst the carbon is oxidized in deeper layers). The nutrient species released upon oxidation or taken up during primary production are equally difficult to define (Brewer and Goldman, 1976) and consequently the alkalinity content of the organic material is uncertain. This is not critical for the construction of the model since the alkalinity fluxes are dominated by the inorganic detritus flux. The detritus to a first approximation contains the same $^{14}C/^{12}C$ ratio as the DIC in the box where the bioproduction takes place. Detritus production is restricted to surface boxes and all detritus is subsequently dissolved in the underlying water column.

4. A 12-box model of the ocean

4.1. *Spatial resolution*

We shall use a 12-box model of the oceans in two versions as shown in Fig. 1 (cf. Bolin, 1983), which is similar to the model proposed by Broecker et al. (1960), but permits better vertical resolution in the major oceans. We may legitimately question some of the results obtained with this very crude representation of the real ocean. More detailed models and particularly the coupling of the present methodology to hydrodynamical models might in the future provide more definite results. As will be seen we shall, however, encounter a number of problems that will be well illustrated with the aid of the present model. The experiences will be useful at later stages when trying to deal with the real ocean in a more realistic manner. Also, a realistic set of advective and turbulent rates of transfer is obtained which is of interest to compare with our knowledge derived in other ways.

We distinguish between the Arctic Ocean, the Atlantic, the Antarctic Ocean and the Pacific/Indian Oceans. In version A the Atlantic, Pacific and Indian Oceans are divided into surface water, intermediate water, deep water and bottom water. In version B, the intermediate water is divided into two layers, while the deep water and bottom water are combined into one abyssal box. In the polar regions, on the other hand, the water below the surface layer is quite homogeneous and is described using single boxes. The Arctic Ocean extends southwards to a line from westernmost Laborador to the south tip of Greenland, Iceland to

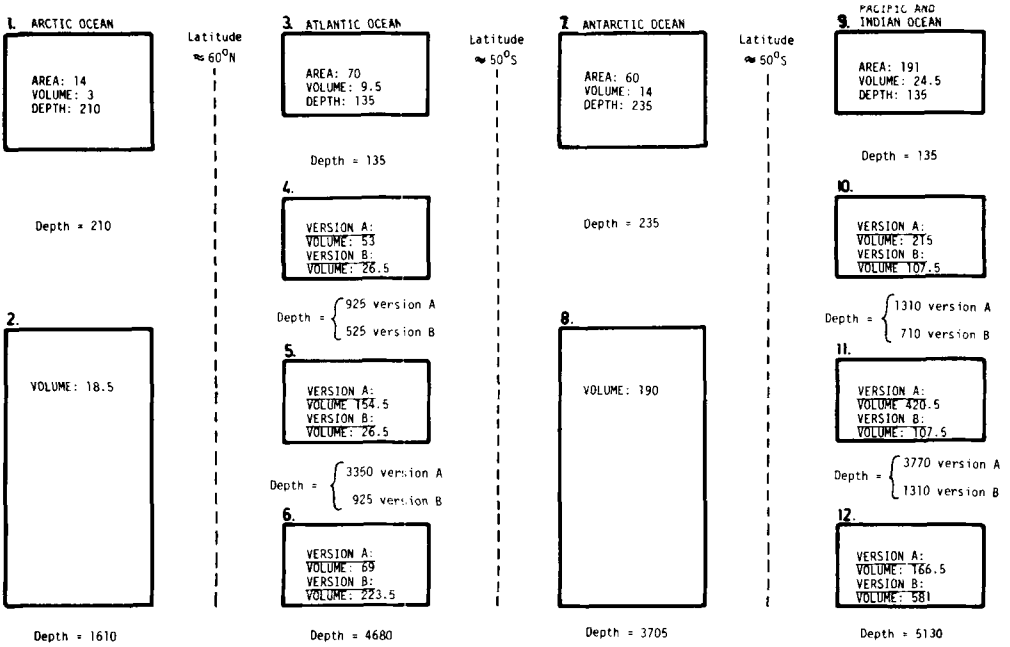

Fig. 1. Box configuration for a 12-box model of the world ocean. Surface areas for the surface boxes are given in 10^{12} m^2, volumes are in 10^{15} m^3 and depths in m. The patterns of advective and turbulent exchange between the boxes are shown in Figs. 7a and 7b for version A and B respectively

northernmost Scotland. The Antarctic Ocean is limited to the area south of the Antarctic Convergence Zone located between 45° S and 50° S. The adjacent seas (except the Arctic Ocean) have not been included. The surface areas, depths and volumes of the boxes are given in Fig. 1.
We have

Version A: $\begin{cases} I = 12 \\ L = 20 \end{cases}$

Version B: $\begin{cases} I = 12 \\ L = 21 \end{cases}$

4.2. *Data*

The GEOSECS program (Takahashi et al., 1981) has provided us with a rich data set for tracer distributions in all major oceans during the years 1972–74. Because of the increase of atmospheric CO_2 during the last 100–200 years and the input of ^{14}C since 1955 the observed distributions of DIC and $\Delta^{14}C$ do not represent a steady state as needed for the present analysis. Not only have the surface layers been influenced, but also the $\Delta^{14}C$ values in the upper part of the intermediate waters (Stuiver, 1980). We shall, however, accept the GEOSECS data for DIC except for the surface reservoirs for which somewhat smaller values have been assigned, the difference being 0.03 mol C m^{-3}. The GEOSECS $\Delta^{14}C$ data have been modified by making use of the early ^{14}C measurements by Broecker et al. (1960). The GEOSECS data for alkalinity, oxygen and phosphorus have been used without modification.

In principle an iterative procedure could be developed to arrive at a better definition of a pre-industrial steady state distribution of DIC and $\Delta^{14}C$ by making use of the transient changes later deduced (Section 6). This warrants further investigation.

Due to malfunction of the titrators during the early stages of the GEOSECS, expedition measurements of DIC and alkalinity are uncertain or lacking for the North Atlantic. We have used the Atlantic averages as given by Takahashi et al. (1981), Table S 5. For the other major oceans data were taken from Tables S 14 (Antarctic Ocean), S 9 (Pacific Ocean) and S 13 (Indian Ocean) in that same publication by Takahashi et al. (1981). Data from the Arctic were obtained from the Swedish YMER expedition as presented by Anderson and Dyrssen (1981).

Average concentrations of the various tracers were deduced using the reported profiles as shown in Figs. 2–6 and an average global hypsographic curve (Table 1). Boxes 9 to 12 include both the Indian Ocean and the Pacific Ocean contributing 29% and 71% respectively to the averages used.

We furthermore require that there is no net CO_2 flux between the atmosphere and the sea for an atmospheric CO_2 pressure of 290 ppm and that there is a difference between the CO_2 partial pressure of the cold surface boxes (1 and 7) and the warm surface boxes (3 and 9), Δp, giving rise to an atmospheric meridional transfer of CO_2 from the equatorial regions towards the poles. In order to satisfy these demands, additional small changes of

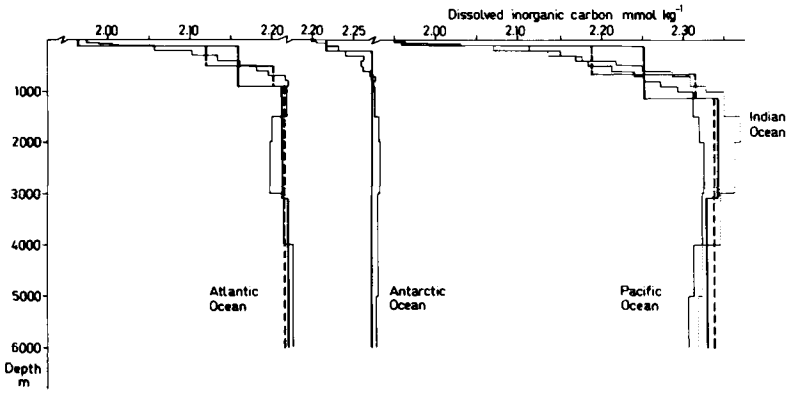

Fig. 2. The observed distribution of dissolved inorganic carbon, q^C (mmol kg^{-1}), as a function of depth in the Atlantic, Antarctic and Pacific Oceans (thin solid line) and the Indian Ocean (dotted line), according to GEOSECS observations as given by Takahashi et al. (1981). The average values assigned for the boxes for version A (heavy solid lines) and version B (dashed lines) are also shown.

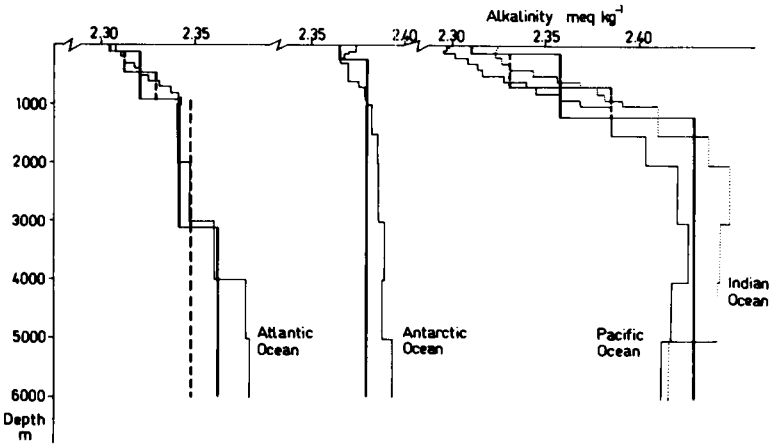

Fig. 3. The same as Fig. 2 but for alkalinity. q^A (meq kg^{-1}).

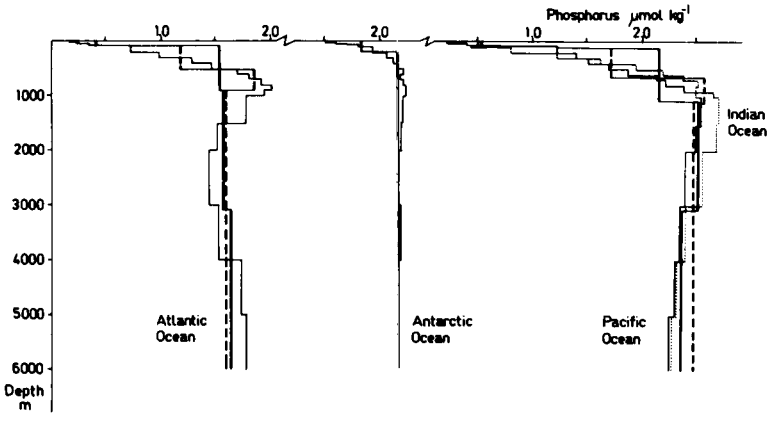

Fig. 4. The same as Fig. 2, but for phosphorus, q^P (μmol kg^{-1}).

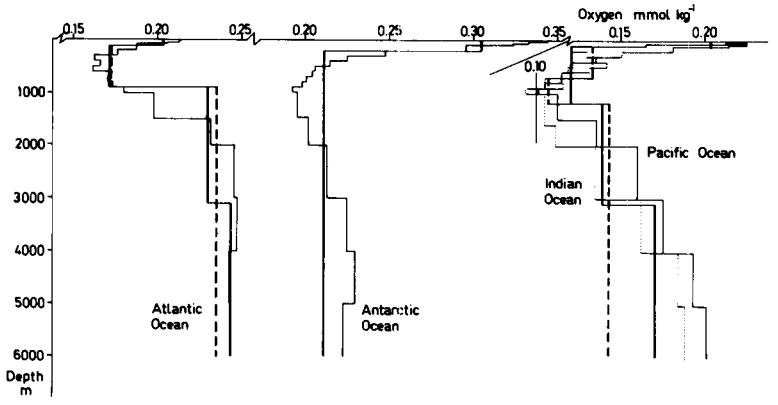

Fig. 5. The same as Fig. 2, but for oxygen, q^O (mmol kg^{-1}).

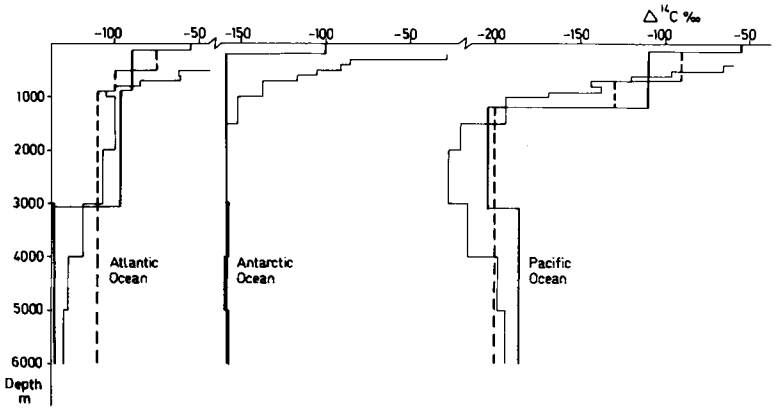

Fig. 6. The same as Fig. 2, but for radiocarbon $\Delta^{14}C$ (‰ departure from standard). Data from Stuiver et al. (1981), but data from the Indian Ocean are not shown. The mean values assigned to the surface boxes have been approximately corrected for the injection of bomb-produced ^{14}C by using data from 1959–60 (Broecker et al., 1960). The difference in $\Delta^{14}C$ values between boxes 5 and 6 in the Atlantic Ocean has been exaggerated by assuming that the depth of the interface between them increases southwards.

Table 1. *Global distribution of ocean depths, derived from the distribution given by Defant (1961) with the exclusion of adjacent seas (except the Arctic Ocean)*

Depth (m)	% of ocean area deeper than this depth
0	100.00
25	100.00
50	99.56
75	99.11
100	98.67
200	96.90
300	96.55
400	96.20
500	95.85
600	95.50
700	95.15
800	94.18
900	94.45
1000	94.10
1500	92.40
2000	90.70
3000	84.50
4000	64.40
5000	27.80

the surface data for DIC were required, partly because of the marked vertical gradient which in reality prevails close to the ocean surface. We have assumed $\Delta p = 30$ ppm in deriving the present initial data set.

Some slight modifications of the values for the different boxes were finally made to ascertain that the total amounts of tracers in the two versions were the same, i.e.

carbon (atmosphere and ocean)	$3100 \cdot 10^{15}$ mol C
alkalinity	$3195 \cdot 10^{15}$ eq
phosphorus	$3.83 \cdot 10^{15}$ mol P

A comparison between the GEOSECS data sets as given by Takahashi et al. (1981) and the average values used in the present computations is shown in Figs. 2–6. Numerical values are given in Fig. 7a (version A) and Fig. 7b (version B).

It should finally be noted that when imposing random disturbances on the variables q_i^m to deduce the importance of an uncertainty in **A** and **b** for our solution, q_i^C and q_i^A must not be perturbed independently; rather we must let one be dependent on the other, subject to the constraint arising from demanding the atmospheric transfer of CO_2 to be specified as above.

The uncertainty in q_i^m is difficult to determine, since it depends both on the accuracy of measurements and how representative the data are for the value q_i^m to be computed. We have assumed that the most appropriate value to use as a box average is found in the range $q_i^m \pm \sigma^m$ where q_i^m is the

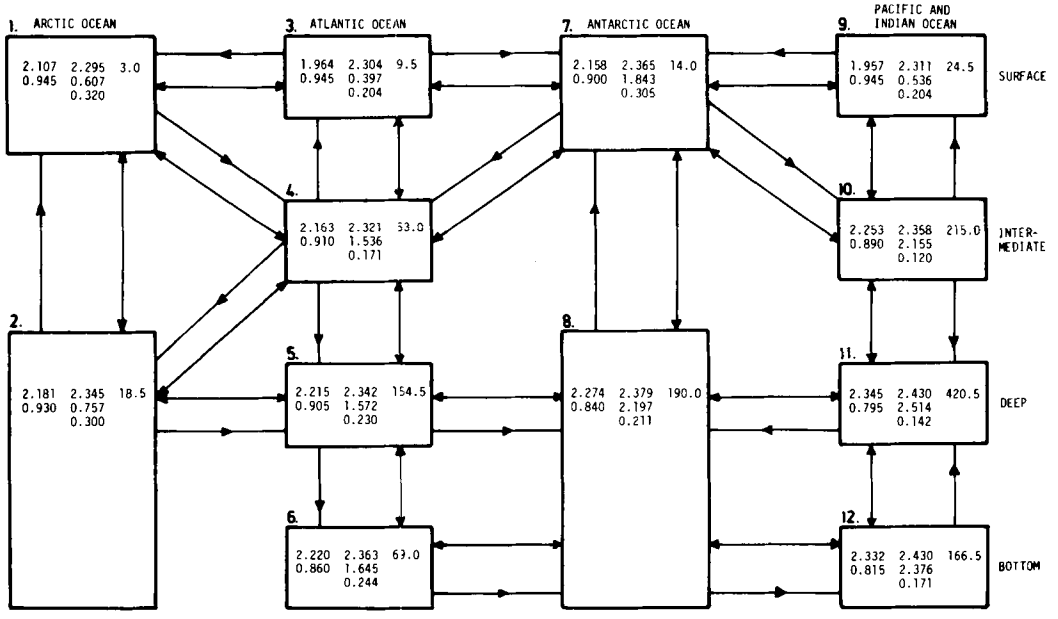

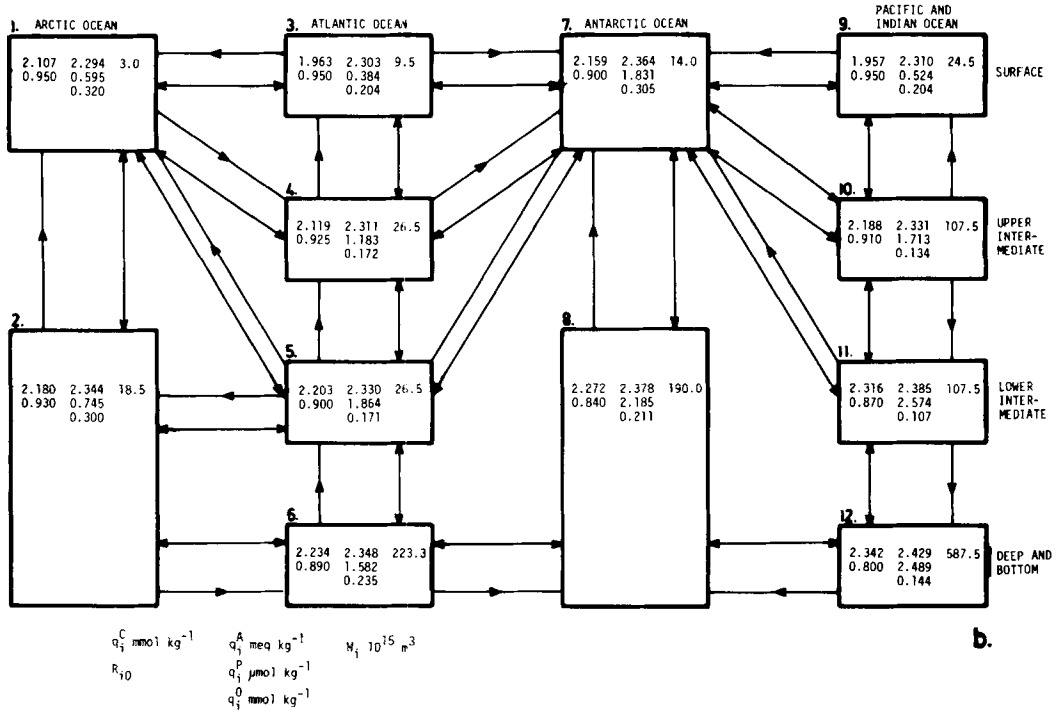

Fig. 7. Concentrations assigned to the boxes and patterns of advective and turbulent exchange for the two versions A (a) and B (b). The variables are ordered in the boxes as shown to the left at the bottom.

concentration as obtained by our averaging procedure and σ^m somewhat arbitrarily have been taken to be:

$$\begin{cases} \sigma^C = 0.01 & \text{mol C m}^{-3} \\ \sigma^* = 0 \\ \sigma^A = 0.004 & \text{eq m}^{-3} \\ \sigma^P = 0.1 & \text{mmol P m}^3 \\ \sigma^O = 0.01 & \text{mol O m}^{-3} \end{cases}$$

4.3. *Computational information*

The reference configuration of the twelve boxes (version A) has twenty common surfaces between boxes. Thus the number of unknowns is $s = 2(20 + 12) = 64$. This is the normal number of columns in the matrix **A**. We have treated two cases in which the numbers of rows, r, are different. Normally we have used five tracers as discussed in Section 3 and thus $r = 12(5 + 1) + 8 = 80$. This system is incompatible and is treated with Method I.

We also have considered the smaller system that arises when the tracers oxygen and phosphorus are omitted, which yields $r = 12(3 + 1) + 8 = 56$. This system, when compatible, is indeterminate. We have used Method II to analyse it.

When using version B in order to investigate the sensitivity of the model to a change of box configuration we have $L = 21$ and thus $s = 2(21 + 12) = 66$. The same 80 equations as in the reference case A were used and we therefore get an incompatible system that was treated with Method I.

To ensure proper scaling of the C-, P- and O-equations (cf. Section 2.3) the concentrations are given in mol m^{-3} and the P- and O-equations multiplied by $(\gamma^P)^{-1} = 106$ and $(\gamma^O)^{-1} = 0.77$ respectively. In the equation for alkalinity we note that q_i^C and q_i^A have about the same numerical values if the units used are mol m^{-3} and eq m^{-3} respectively. No scaling of the A-equation therefore seems necessary. For ^{14}C we use the concentrations $q_i^* = q_i^C \cdot R_{io}$, where R_{io} has been defined in eq (3.1). Since R_{io} is close to unity, q_i^* is of nearly the same magnitude as q_i^C which ensures equal weighting of the C- and ^{14}C-equations. The water continuity equations, finally, are tuned to the rest of the system by multiplication with a constant of 2 moles m^{-3}.

The solution for this system was not satisfactory, because the ^{14}C-equations did not carry sufficient weight to ascertain a proper turnover time for the system. Since the tracers of carbon (C, ^{14}C, A) are closely interlinked the weights for all these equations were increased simultaneously with one and the same factor, which was also applied to the continuity equations for water. As larger values of this factor are chosen, more realistic rates are obtained, but beyond a value of 10 the solution does not change much. A scaling factor of 25 was finally adopted. This scaling procedure can be interpreted as follows. The equations for C, ^{14}C, A and water constitute a system with fewer equations than unknowns. There are therefore an infinite number of solutions (or, if the system is incompatible, an infinite number of least-square approximations). Among those we choose one that minimizes the sum of squares of the residuals for the P- and O-equations. For the final solution 82% of the total sum of squares stem from the P-equations, 16.5% from the O-equations and less than 2% is due to the C, ^{14}C, A and water equations.

A steady state solution obtained is very close to a steady state for the given data for C and ^{14}C. We are interested in studying the transient behaviour of the model subject to external sources of carbon (fossil fuel emissions) and ^{14}C (bomb-produced ^{14}C). To do so the initial steady state must be well established. Our choice of solution satisfies this requirement adequately.

It is important to determine the uncertainty of the solutions obtained. To do so ten additional solutions were determined in which cases the data fields were perturbed in a random manner with the root mean square errors as given in Section 4.2. The variability of these solutions around the mean solution are shown in the following.

In the process of obtaining a solution for the tracer distribution shown in Fig. 7a (version A), we first deduced the unconstrained least-square solution ($\mathbf{A}\mathbf{x}_p = \mathbf{b}_p$, cf. Section 2.2 and Appendix). Thirteen of the turbulent exchange coefficients were positive and all F_{oi} and F_{ci}, i.e. the organic and inorganic detritus transfers, had the correct sign. When enforcing the constraint $\mathbf{G}\mathbf{x} \geq \mathbf{h}$ the preliminary solution changes to x_d. The characteristic features of the solution, however, do not change fundamentally, except that all turbulent exchange coefficients of course become zero or positive as prescribed. As a matter of fact, seven values become zero, but only five of those were negative in the unconstrained solution. The average of the ten perturbed solutions differs little from the

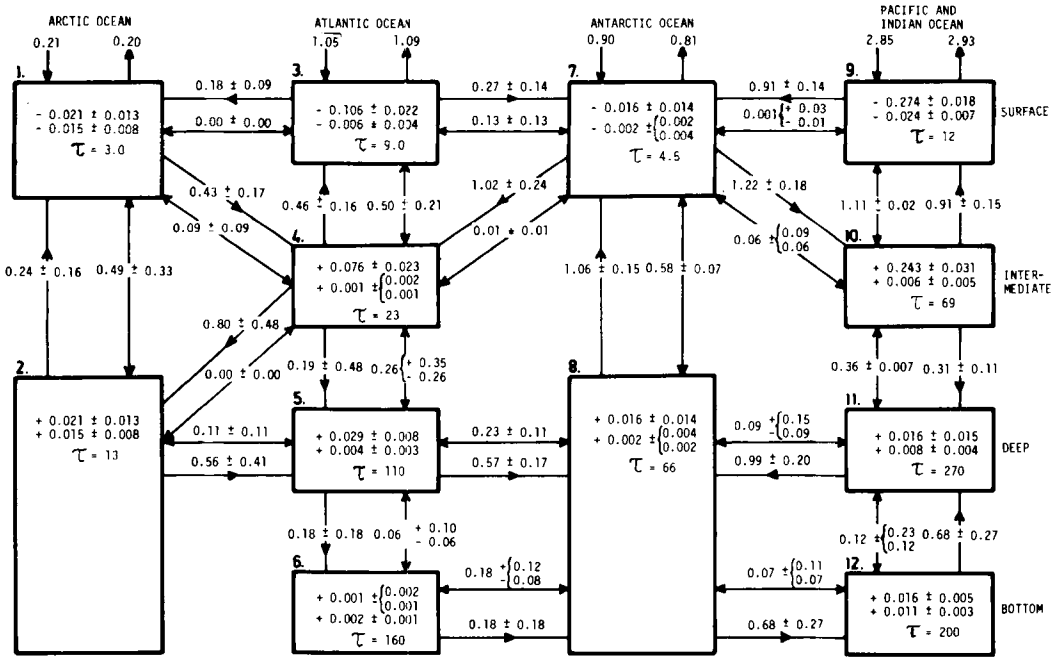

Fig. 8. Deduced fluxes for model version A (reference case). Between boxes: advective (→) and turbulent (↔) fluxes of water (10^{15} m^3 yr^{-1}). Flow into or out from boxes 10^{15} mol C yr^{-1}. In boxes: net organic detritus formation and loss of carbon (–) or decomposition and gain of carbon (+) in 10^{15} mol C yr^{-1} (upper line), net carbonate formation and loss of carbon (–) or dissolution and gain of carbon in 10^{15} mol C yr^{-1} (middle line), and turnover time (τ) for water in the box (lower line).

solution based on the data field given in Fig. 7a. We note, however, that only three of the turbulent exchange coefficients are zero in all ten experiments (between boxes 1–3, 2–4 and 7–9), but altogether eleven mean values for these coefficients are not significantly different from zero (Fig. 8). Essentially the same results hold for solutions for the version B of the model.

Details of the computational procedure are given in the Appendix. The program was executed on a CD Cyber 170–720 using double precision.

5. Analysis of steady state solutions to the 12-box model

5.1. *Solution for the reference case (version A)*

A solution was computed with the reference data. In order to explore the uncertainty due to errors or lack of representativity in the data, ten additional solutions were derived, where perturbations were added to the tracer concentrations. In perturbation experiment number $j, j = 1, 2, \ldots 10$, the tracer concentrations were set to

$$q_{ij}^m = q_i^m + z_{ij}^m \sigma^m$$

where q_i^m is the reference value, σ^m is as described in section 4.2, and the numbers z_{ij}^m are independent samples of a gaussian random variable with zero mean and unit standard deviation.

Fig. 8 shows the resulting mean values for all the unknowns, and the observed standard deviations. We note the following important features.

Turbulent exchange plays about as important a role as advection between surface boxes and the layer below (i.e. 1–2, 3–4, 7–8, 9–10). Also turbulence between intermediate water and the deep water in the Pacific/Indian Ocean is significantly different from zero, but still comparatively small in view of the large area occupied in comparison with the Atlantic and the Antarctic Oceans. Otherwise the steady state distribution of tracers in the abyssal sea is primarily maintained by advective motions and detritus fall. It is

interesting to note that the five turbulent exchange coefficients that are significantly different from zero in the final solution are positive already in the unconstrained solution. The negative values obtained in that case thus seem primarily due to the crude resolution of the model and the difficulty of assigning proper values for the concentrations q_l^m.

There are four sets of major circulations that describe 80–90% of the advective flow in the model (see Fig. 8).

$$7 \rightarrow 4 \rightarrow 2 \rightarrow 5 \rightarrow 8 \rightarrow 12 \rightarrow 11 \rightarrow 8 \rightarrow 7$$
$$1 \rightarrow 4 \rightarrow 3 \rightarrow 1$$
$$7 \rightarrow 4 \rightarrow 3 \rightarrow 7$$
$$7 \rightarrow 10 \rightarrow 9 \rightarrow 7$$

The first one represents the major circulation of the combined Atlantic/Pacific/Indian Oceans. It presumably is obtained as a result of the gradual increase of q^C, q^Δ and decrease of q^* when proceeding from the Atlantic deep water (5) through the Antarctic deep water (8) into the Pacific/Indian bottom water (12) and up through the Pacific/Indian deep water (11). The three following circulations are characteristic for the maintenance of the thermocline region. Qualitatively the pattern agrees with the overall circulation of the oceans (cf. Gordon, 1971).

Antarctic net upwelling is $1.06 \cdot 10^{15}$ m^3 yr^{-1} = 32 Sv. This should be compared with the value $1.2 \cdot 10^{15}$ m^3 yr^{-1} $\pm$ 38 Sv that is obtained by Gordon (1971) as the difference between the upwelling due to Ekman drift northward, $1.7 \cdot 10^{15}$ m^3 yr^{-1}, and the deep water formation near the Antarctic continent, $0.5 \cdot 10^{15}$ m^3 yr^{-1}.

Down welling from Antarctic surface water into the Intermediate waters of the Atlantic and Pacific/Indian Oceans, about 35 Sv, is also in reasonable agreement with other estimates (Gordon, 1971).

The solution shows weak advective flow from the Atlantic deep water into the bottom layer and further into the Antarctic deep water. This is opposite to the common view of Atlantic bottom water formation, but the computed value is not significantly different from zero. The advective flow is not determined very accurately ($0.18 \pm 0.18 \cdot 10^{15}$ m^3 yr^{-1}) and the model resolution does not permit a more definite conclusion regarding the rate of renewal of Atlantic bottom water. The rate of advective flow from Antarctic deep water into the bottom layers of the Pacific/Indian Ocean $0.7 \cdot 10^{15}$ m^3 yr^{-1} agrees well with estimates of $0.6 \cdot 10^{15}$ m^3 yr^{-1} by Munk (1966).

The upwelling from intermediate waters into the surface waters in the Atlantic and Pacific/Indian Oceans corresponds to 7 and 5 m yr^{-1}. To convert the values for turbulent exchange into eddy exchange coefficients (cf. Section 2.1) we assign a value $\Delta_{3,4} = \Delta_{9,10} = 500$ m and obtain a value $K_z \approx 1$ cm^2 s^{-1}, which is less than commonly accepted for the surface layer but approaching the value valid for the thermocline region (Munk, 1966).

The turn-over time of water in the Arctic deep basin seems unreasonably short. It is primarily a result of the rather high value assumed for $\Delta^{14}C$ in the Arctic deep water (0.93) in comparison with the value 0.91 assigned to the Atlantic intermediate water. A value merely 0.01 or 0.02 less would significantly decrease the rate of Arctic deep water formation. Further experimentation should be made using more abundant ^{14}C data now becoming available (I. Ohlsson, personal communication). Extrapolation to pre-bomb conditions would still introduce uncertainty.

The total detritus flux from the surface waters into the intermediate and abyssal sea, $(5.0 \pm 0.5) \cdot 10^{15}$ g C yr^{-1} and $(0.6 \pm 0.2) \cdot 10^{15}$ g C yr^{-1} for organic and inorganic carbonate matter, is not very sensitive to errors in the data fields. The ratio, about 8 : 1, agrees well with observations at the top of the thermocline region (cf. Chen, 1978). The small values for the detritus fluxes in the Antarctic Basin are not realistic. The vertical profiles of bacterial decomposition of organic matter with a maximum in the intermediate waters and of chemical dissolution of carbonate shells with a maximum in the deep or bottom waters, agree qualitatively with other estimates (Wyrtki, 1962).

In spite of the fact that the rate of CO_2 exchange between the atmosphere and the sea has been assumed to be the same for all surface reservoirs for a given CO_2 partial pressure difference, more than 50% of the net flux of ^{14}C from the atmosphere into the oceans takes place in the Antarctic Ocean, the area of which is less than 20% of the total ocean area (cf. Fig. 1). This is a result of the comparatively low value for the CO_2 partial pressure in these waters and the large $\Delta^{14}C$ difference across the air–sea interface. It seems likely that this finding is even more pronounced in reality, since the transfer probably depends on the wind velocity (Liss, 1983), and therefore probably

is enhanced in the latitudes of strong winds around the Antarctic. Peng et al. (1979) have determined the rate of CO_2 exchange between the atmosphere and the sea by studying the rate of Radon evasion. They found appreciably higher values around the Antarctic than at low latitudes. This result, however, critically depends on normalization of their data to a standard temperature of + 20° C, while the rates at prevailing temperatures should rather be used in the present case. Further, their analysis is based on an assumption that the depth of the thermocline does not depend on the wind velocity, which is hardly acceptable. In order to analyse the sensitivity of the results to this and some other assumptions, a few further experiments were made, as discussed below.

5.1.1. *Enhanced air–sea exchange in the Antarctic Ocean*

We explore the implications of an assumption that the rate of CO_2 exchange per unit area and per unit pressure difference between the atmosphere and the sea in the Antarctic Ocean is twice that at lower latitudes. This may be excessive, but will clarify the significance of this pathway. The flux pattern is shown in Fig. 9. More than 70% of the net transfer of ^{14}C occurs into the Antarctic Ocean. The increased air–sea exchange also requires more rapid exchange at greater depth both in the Antarctic and the Pacific/Indian Oceans. Finally, the detritus flux in the Antarctic Ocean is increased in comparison with the reference case.

5.1.2. *Decreasing $\Delta^{14}C$ for the Antarctic surface reservoir*

The Antarctic surface reservoir plays an important role by interconnecting all major oceans. Very few ^{14}C measurements were made before bomb-produced ^{14}C markedly contaminated the ocean surface water. To explore the sensitivity of our results to the choice of the value $R_7 = 0.90$ another solution has been determined with $R_7 = 0.87$, while all other tracer concentrations have been left unchanged. Admittedly this value most likely is too low but the sensitivity of our solution to the $\Delta^{14}C$ value for this water mass is well illustrated. The solution is given in Fig. 10. We note rather large changes in the values for the fluxes. Considering the uncertainty derived for the transfers in the reference case, we find a significant difference between the present solution and that for the reference case (i.e. a shift greater than twice the standard deviation) for only the Antarctic and Pacific/Indian Oceans. Particularly we note the much increased vertical turbulent exchange in the Antarctic and the larger rates of detritus flux.

5.1.3. *The sensitivity of the solution to the choice of Redfield ratios*

The values for γ^m used in the computations described above were those given by Redfield (1958), as given in Section 3.3. In reality fractionation may, however, occur in the decomposition process. We have therefore asked the question: Which values for the Redfield ratios should be used in order to minimize the errors in attempting to satisfy the tracer equations? Even though the search for a minimum error was not quite completed we find that the total error is reduced by more than 40% by changing $(\gamma^O)^{-1}$ from –0.77 to –0.65 and $(\gamma^P)^{-1}$ from 106 to 70. While the errors in the C, A and water equations are slightly increased and those of the ^{14}C-equations, somewhat decreased, a significant improvement is achieved in how well the P and O equations are satisfied. The errors of the latter still constitute 77% and 18% respectively of the total error, compared with 82% and 16.5% for the reference case. As seen from Fig. 11 the flux pattern is hardly changed. Only the advection through the Pacific/Indian bottom water is increased significantly. The decrease of both ratios implies that C would be preferentially dissolved in the surface layer before the detrital matter settles into deeper strata and dissolves there. This finding is contrary to the general view regarding fractional decomposition of organic matter (Chen and Pytkowicz, 1979). It is likely that the spatial resolution is much too crude to permit a conclusive analysis of this problem with the present model. The experiment should therefore be considered as a demonstration of the possibility to use this method of analysis rather than a "proof" that fractionation occurs in the processes of bacterial decomposition of organic matter in the sea.

5.2. *Solution for box configuration according to version B*

It was pointed out previously that the spatial resolution may influence the results. We have analysed this possibility by deriving a solution for

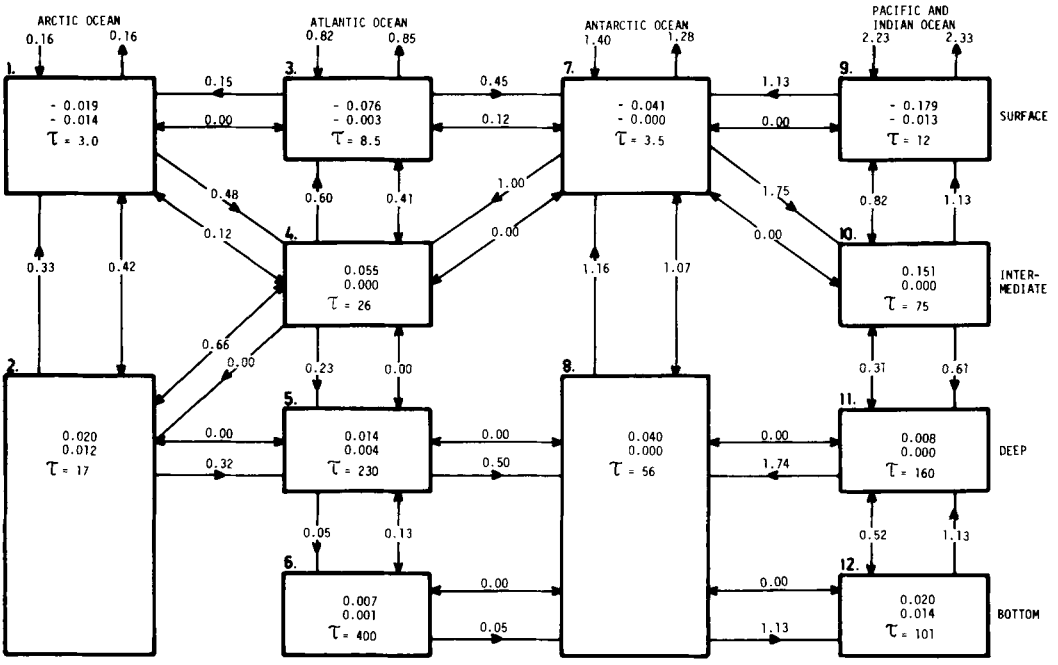

Fig. 9. Deduced fluxes for model version A, but rate or air–sea exchange per unit area between atmosphere and sea 100% larger for surface reservoir 7 (Antarctic) than for the other surface reservoirs 1, 3 and 9. Notation as in Fig. 8.

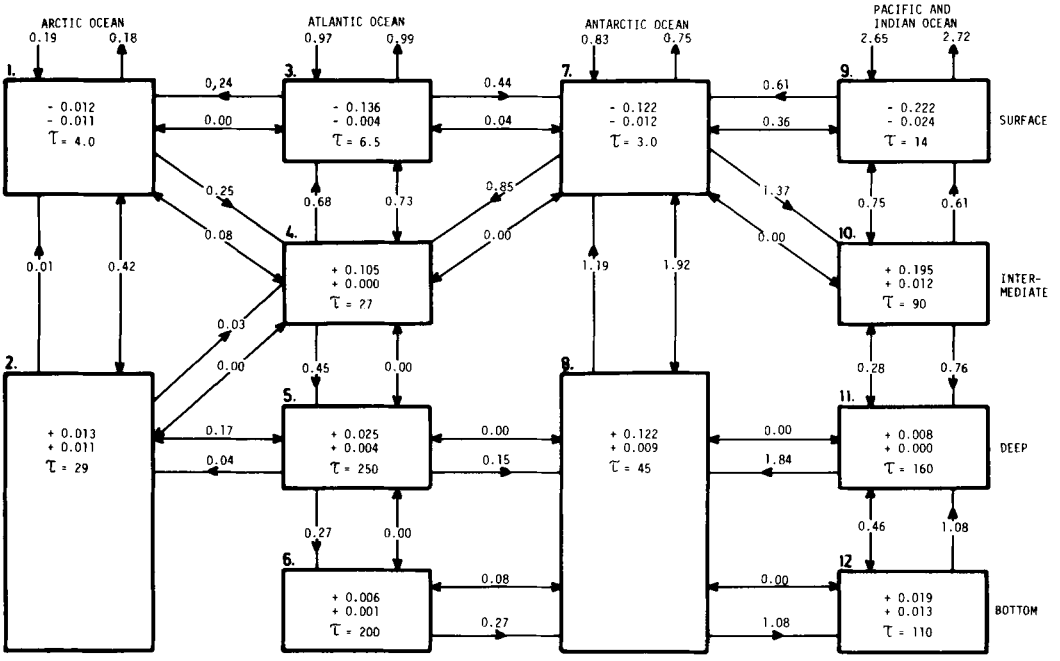

Fig. 10. Deduced fluxes for model version A, but $R_7 = 0.87$ rather than 0.90 as used in the reference case shown in Fig. 8. Notation as in Fig. 8.

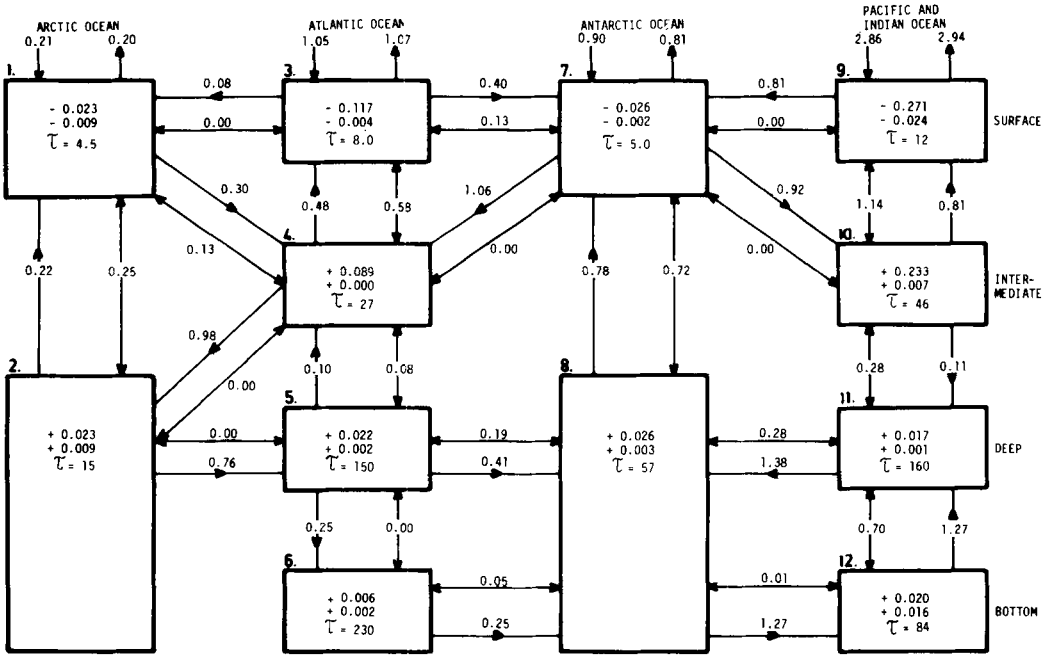

Fig. 11. Deduced fluxes for model version A, but different Redfield ratios, $(\gamma^{O})^{-1} = 0.65$ (rather than 0.77 in the reference case) and $(\gamma^{P})^{-1} = 70$ (rather than 106). Notation as in Fig. 8.

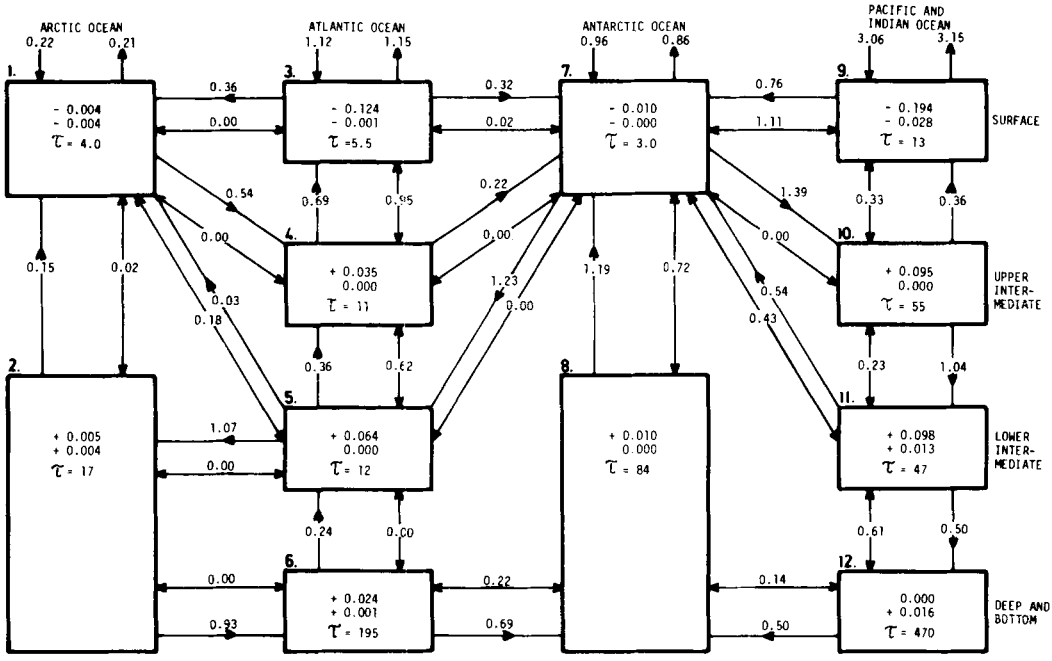

Fig. 12. Deduced fluxes for model version B. Notation as in Fig. 8.

the box configuration shown in Fig. 1b and the data as given in Fig. 7b. The tracer fields in reality are characterized by strong gradients in the upper layers, while the distributions are much more homogeneous in the abyssal sea. For this reason the vertical resolution in upper layers was increased by dividing the intermediate waters in the Atlantic and Pacific/Indian Oceans in two layers and combining the deep and bottom waters in these basins into single reservoirs. The solution is shown in Fig. 12.

We first note that the general features of the solutions for the two different spatial configurations are the same. This can be made clear by some comparisons. In the Atlantic Ocean, we consider boxes 5 and 6 (in version A) as one combined reservoir, compute the exchanges between this combined reservoir and its surroundings, and compare the results with the transfers to and from box 6 in version B, which represents the same body of water. An analogous comparison can be made in the Pacific/Indian Ocean. Furthermore, corresponding comparisons between the exchanges between the single intermediate reservoir and the surroundings in version A and the divided reservoirs in version B also show great similarities.

There are considerable differences in the turnover times but these are mostly dependent on the changed box configurations. There are essentially three noticeable differences between the two solutions.

The advective flux from Atlantic intermediate water (Version A, box 4; Version B, box 5) into the Arctic deep basin (2) and back to the Atlantic deep water (Version A, box 5; Version B, box 6) is twice as intensive in version B as in version A. As pointed out before, there is considerable uncertainty in the determination of the advective flux into and out of box 2.

Conversely the circulation from Antarctic surface water to Pacific/Indian intermediate water to Pacific/Indian surface water and back to the Antarctic is about twice as strong in version A as in version B. This change is associated with a considerable reduction in the intensity of turbulent exchange between the surface and intermediate waters in the Pacific/Indian Ocean. This difference warrants a closer analysis, which is, however, beyond the scope of the present paper.

The flux of both organic and inorganic matter is reduced by about 20% in version B. The distribution between the four surface reservoirs is also somewhat changed.

We also note some interesting features of the more detailed distribution of fluxes in the intermediate waters of the Atlantic and Pacific/Indian Oceans in version B. The down-welling from the Antarctic surface waters penetrates into the lower intermediate layer in the Atlantic Ocean (box 5) and into the upper one in the Pacific/Indian Ocean (box 10). Further the decomposition of organic detritus occurs at more shallow depths in the Pacific/Indian Oceans, even though the difference in our results between the two major oceans in this regard may not be significant. The result presumably depends on the fact that the vertical gradients are steeper in the Pacific/Indian Oceans than in the Atlantic (cf. Figs. 2–6).

The results of this comparison can be taken as indicative of the uncertainty of the results as dependent on box configuration and spatial resolution, even though the crucial test obviously would be to increase the resolution throughout the ocean.

5.3. *Solution to model version A when omitting phosphorus and oxygen as tracers*

The version A of the model has 66 unknowns and the omission of phosphorus and oxygen as tracers reduces the number of equations to 56. The reference data (Fig. 7a) yield an indeterminate system, that can be uniquely solved if demanding physical realism and minimizing $\|\mathbf{x}\|$ (Method II as described in Section 2.2). When the data field was perturbed, the system remained indeterminate, but there did not always exist an exact solution with correct signs on all the unknowns. Performing 50 perturbation experiments, we obtained successful results in 16 cases. Except in the following important aspect the average of these altogether 17 solutions, within the range of uncertainty, is the same as previously derived when also making use of phosphorus and oxygen (compare Figs. 8 and 13).

An analysis of the advective fluxes and turbulent exchange rates between boxes 7, 9 and 10 shows that the solutions fall into three different classes:

(i) Eight solutions are similar to the average solution obtained when also using phosphorus and oxygen as tracers (see Fig. 8). The average of these eight solutions is shown in Fig. 13.

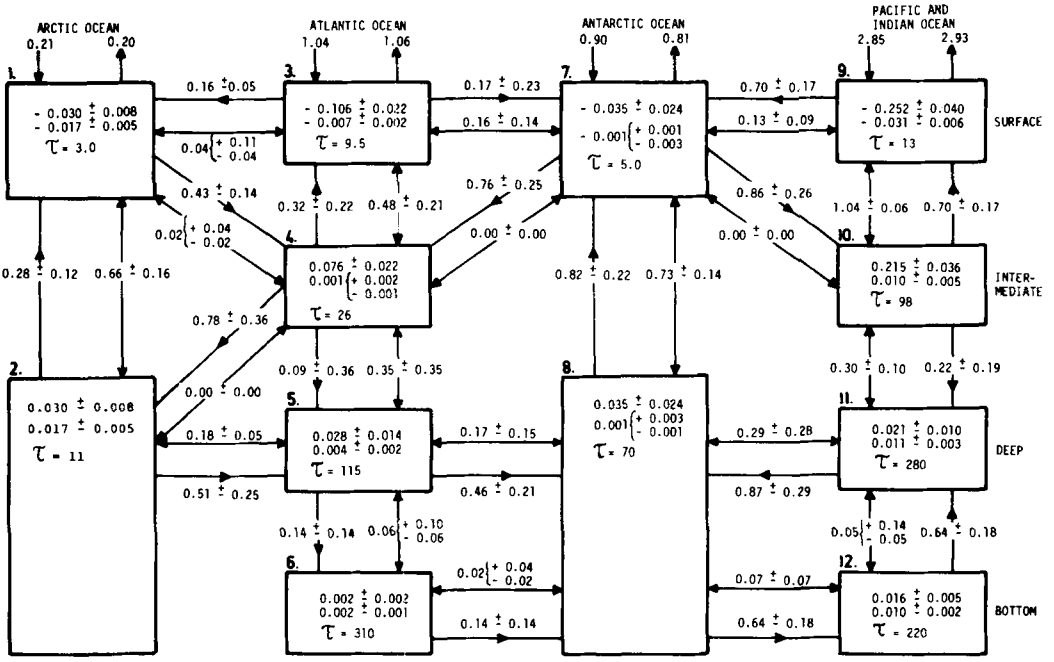

Fig. 13. Deduced fluxes for model version A, but with omission of phosphorus (P) and oxygen (O) as tracers. The figure displays the average of eight solutions of class (i), which are similar to the reference case (cf. text). Notation as in Fig. 8.

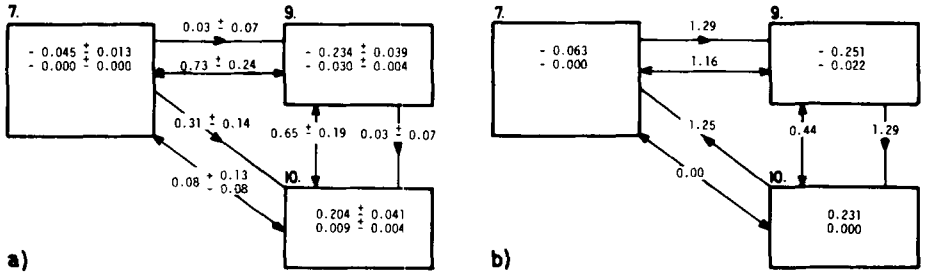

Fig. 14. Deduced fluxes for model version A, but with omission of phosphorus (P) and oxygen (O) as tracers, class ii solution (a), and class iii solution (b) for the reservoirs 7, 9 and 10 while other fluxes are not significantly different from those shown in Fig. 13.

Even though somewhat weaker a circulation 7 → 10 → 9 → 7 prevails (cf. Fig. 8).

(ii) Eight other solutions on the average show no net circulation through the three reservoirs 7, 9 and 10. The turbulent fluxes are also different as shown in Fig. 14a.

(iii) One solution is characterized by a strong circulation in the opposite direction, i.e. 7 → 9 → 10 → 7 as shown in Fig. 14b.

The reference solution and (i) above, in principle, agree with the common view of the general circulation of the oceans. It is then interesting to note that the solutions (ii) and (iii) are not compatible with the distributions of phosphorus and oxygen, which are used to deduce the reference solution. As a matter of fact, inclusion of phosphorus and oxygen equations seems to eliminate solutions of type (ii) and (iii). The reference

solution is remarkably stable in this regard. The turbulent exchange of water between boxes 9 and 10 is $1.11 \pm 0.02 \cdot 10^{15}$ m^3 yr^{-1}, i.e. an uncertainty of merely 2%.

6. Transient behaviour of the 12-box model

6.1. *Formulation of the experiments*

Within the framework of the models adopted we have derived some gross features of the quasi-steady state ocean circulation, detritus formation and decomposition which are consistent with given sets of tracers. The tracer distributions were chosen to represent pre-industrial conditions even though they primarily were based on measurements from the GEOSECS expeditions during the years of 1972–74. Approximate corrections were applied to account for the increases of radiocarbon due to nuclear bomb testing.

Assuming that these circulation patterns and detritus fluxes have not changed since man-made emissions began, we can compute the transient behaviour of the carbon cycle in the sea due to external disturbances. The results may be compared with observations of the transient behaviour of the carbon system in the sea, primarily that of ^{14}C. It is important to emphasize, however (cf. Fiadeiro, 1983), that our model is not capable of reproducing adequately transient processes that are more rapid than the characteristic response times of the boxes, of which the model is composed. The turnover times, as given in Figs. 8–13, show that the rather small surface boxes possibly can reproduce changes with characteristic time-scales of about a decade, but the deeper layers respond more slowly. The emissions of CO_2 have been increasing rather slowly, approximately exponentially with an e-folding time between 20 and 30 years. The input of ^{14}C to the atmosphere by nuclear explosions was large during a limited period between 1958 and 1963. It is therefore likely that the transfer of CO_2 into the sea is better accounted for than that of ^{14}C. Even though a model with better spatial and thereby also temporal resolution will thus be required, some interesting results are obtained. We also note some other difficulties inherent in experiments of this kind.

The emissions of CO_2 to the atmosphere due to fossil fuel combustion are quite well known since 1860 (Rotty, 1981). It is likely that considerable emissions due to deforestation and expanding agriculture have also occurred during this period of time (Moore et al., 1981). These latter emissions are, however, much less accurately known. In this first series of time integrations we will be content in trying to derive the ocean response to emissions due only to fossil fuel combustion. Even though we cannot in this way reproduce reality very well, it is of interest to deduce the airborne fraction of the given emission and the magnitude of the Suess effect (i.e. the change of ^{14}C/^{12}C ratio due to fossil fuel emissions) and compare the latter result with observed values before man-made emissions of ^{14}C began in 1955.

The emissions of ^{14}C to the atmosphere due to nuclear bomb testing are not well known, but the actual changes of Δ^{14}C in the atmosphere during the period 1954 until today have been carefully recorded (e.g. Nydal et al., 1979). We shall therefore prescribe the Δ^{14}C value for the atmosphere as observed, deduce the flux into the oceans using the present model and compare the computed Δ^{14}C values for the surface reservoirs with those observed during the period 1955–73.

As was already briefly referred to in Section 4.3, we encounter a principle difficulty when carrying out such time integrations. The individual steady state equations of the set (2.9) are not identically satisfied, since the set is incompatible and the norm $\|\mathbf{Ax} - \mathbf{b}\|$ is minimal but not exactly zero. Thus the term $\partial q^m/\partial t$ in the time dependent equations (2.1) is not equal to zero for the given tracer distributions, nor is the continuity equation (2.2) identically satisfied. Only very slight changes of the advective fluxes v_{ij} are required in order to have the continuity equation (2.2) for water satisfied, which is easily accomplished. We may next deduce the steady state distributions of our set of tracers, which is compatible with the deduced transfer rates, by a time integration over a sufficiently long time without any external sources or sinks. In minimizing $\|\mathbf{Ax} - \mathbf{b}\|$ the equations for carbon, radiocarbon, and alkalinity have been given more weight. For this reason also the changes of these tracer distributions to achieve steady state are small. The correlations between given tracer fields and those deduced as steady states are 0.981, 0.999 and 0.991, respectively, in the reference solution for version A and 0.983, 1.000 and 0.999 for the corresponding solution in version B. The oxygen

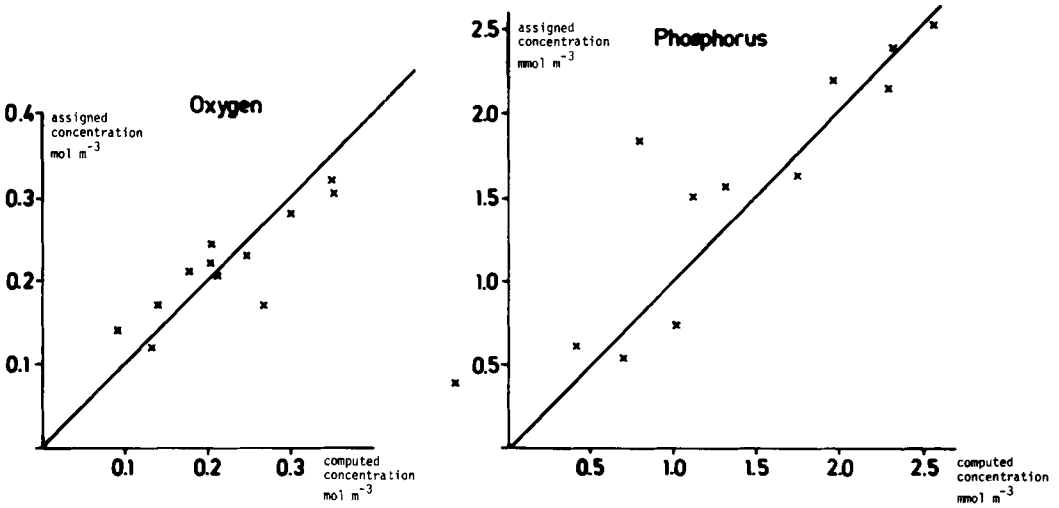

Fig. 15. Scatter diagram of assigned concentrations versus computed concentrations for the twelve boxes in reference case (A), the latter obtained by time integrations to steady state.

and phosphorus equations, on the other hand, are much less well satisfied. More significant changes of these two tracer fields are required in order to satisfy the requirements for a steady state. For this reason the correlation coefficients between the assigned and computed tracer fields are smaller, being 0.863 and 0.895 respectively for version A and 0.813 and 0.914 for version B. Scatter diagrams for the assigned and computed values for oxygen and phosphorus are shown in Fig. 15. It should be remarked, however, that the model is static in the sense that the detritus formation, decomposition and dissolution have been assumed to be independent of the abiotic factors. In reality the rate of photosynthesis, for example, and thus detritus formation is dependent on the phosphorus availability in the surface boxes. Such a more adequate description of these biological processes is beyond the scope of this paper but must of course be considered in later attempts to develop the present methodology further.

Starting from steady states deduced as indicated above, time integrations have been performed for the time period 1860 to 1980 with carbon dioxide emissions into the atmosphere in accordance with the statistics compiled by Rotty (1981) and prescribed ^{14}C concentrations for the atmosphere since 1955 as given by Tans (1981).

6.2. *Ocean response to atmospheric CO_2 emissions*

Table 2 shows the computed changes of q_i^c in the atmosphere and the ocean reservoirs for the period 1860–1980 and the associated changes of $\Delta^{14}C$, the Suess effect, 1860–1955, i.e. until bomb-produced ^{14}C was emitted into the atmosphere. The differences between the two versions A and B are hardly significant. Fig. 16 shows the changes of atmospheric CO_2 partial pressure as computed with version A of the model from 1860 to 1980 and the observed changes at Mauna Loa during the last 22 years according to Bacastow and Keeling (1981).

The computed air-borne fraction of the CO_2 emissions during the period 1959–80 was 74–75% for both versions A and B, while the observed value according to Bacastow and Keeling (1981) was 55%, if it is assumed that no net emissions from the terrestrial biosphere has taken place. We recall, however, that probably a considerable net transfer of carbon to the atmosphere has occurred because of deforestation and expanding agriculture which implies that the airborne fraction of emissions to the atmosphere in reality has been considerably less than 55%.

The computed Suess effect in 1955 is −3.7‰, while the observed value is about −2‰ (Keeling, 1973; Stuiver and Quay, 1981). This discrepancy is partly due to the fact that no net exchange of ^{14}C with the terrestrial biosphere has been included into the model. It seems clear, however, that the oceanic uptake of CO_2 and $^{14}CO_2$ is less in the model than in reality.

Table 2. *Transient changes of q_i (in mol m^{-3}) and $\Delta^{14}C$ (in %)*

	Version A (Fig. 8)			Version B (Fig. 12)		
	Change of q_i^c 1860–1980 mol m^{-3}	Suess effect 1955 %	Change of $\Delta^{14}C$ 1955–1974 %	Change of q_i^c 1860–1980 mol m^{-3}	Suess effect 1955 %	Change of $\Delta^{14}C$ 1955–1974 %
Atmosphere	—	−3.7	—	—	−3.7	—
Ocean reservoirs						
1	0.024	−0.9	+11.1	0.028	−1.5	+19.7
2	0.009	−0.5	+ 1.4	0.009	−0.4	+ 0.2
3	0.032	−1.5	+20.8	0.033	−1.4	+16.2
4	0.011	−0.5	+ 2.4	0.015	−0.8	+ 3.8
5	0.002	0.0	+ 0.0	0.015	−0.7	+ 4.1
6	0.000	0.0	+ 0.0	0.001	−0.0	+ 0.0
7	0.028	−1.1	+18.6	0.027	−1.0	+17.3
8	0.000	0.0	+ 0.0	0.001	−0.0	+ 0.1
9	0.032	−1.4	+21.0	0.035	−1.7	+25.7
10	0.005	−0.3	+ 1.1	0.005	−0.3	+ 1.2
11	0.000	0.0	+ 0.0	0.001	−0.0	+ 0.2
12	0.000	0.0	+ 0.0	0.000	−0.0	+ 0.0
Airborne fraction						
1980	72.0%			73.1%		
1959–1980	74.2%			74.9%		
ΔP_{CO_2} 1860–1980	55 ppm			57 ppm		

The sensitivity of the computed air-borne fraction to uncertainties in the data field has been analysed by performing time integrations with all 17 solutions that were deduced with the reduced set of equations (i.e., without oxygen and phosphorus) as described in Section 5.3. For both the solutions of class (i) and (ii) we obtain 73.0 ± 1.5%, while the single solution of class (iii) gave a value 74.4%. The uncertainty of the determination of the airborne fraction due to errors in the data field is 1–2%, but there is a considerably greater uncertainty due to the choice of model structure as will be discussed below.

Time integrations have also been performed using the transfer fields which were based on enhanced rates of air–sea exchange in polar regions and lower value for $\Delta^{14}C$ in the Antarctic surface water (cf. Section 5.1.1 and 5.1.2). In both cases the airborne fraction was reduced by a few per cent.

The value for the airborne fraction obtained in these computations most likely represents an upper limit. The rather crude resolution of the ocean decreases the efficiency of the oceans as a sink. Generally, one big reservoir responds more slowly to a rapidly changing disturbance than do a number of small reservoirs having the same total volume and average ^{14}C age and being in exchange with each other. With the aid of the diagrams published by Bacastow and Björkström (1981), the airborne fraction of a 2-box model with the same depth of the mixed layer as the mean for the present model (≈150 m) and average value for the deep sea $R_{lo} = 0.84$ is 78%. A box diffusion model yields less than 65% primarily because of a more effective transfer by diffusion into the upper layers of the deep sea than is accomplished by first-order exchange processes in the two-box model. Viecelli et al. (1981) have modified the box-diffusion model by permitting much more rapid downward transfer

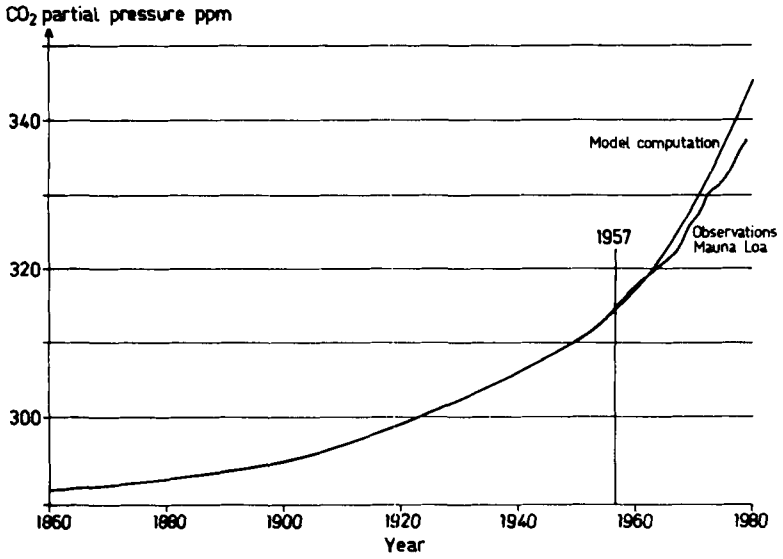

Fig. 16. Computed change of atmospheric CO_2 (using model version A) during period 1860–1980, due to fossil fuel emissions as estimated by Rotty (1981). Lower curve from 1957 to 1979 shows the observed changes at Mauna Loa, according to Bacastow and Keeling (1981).

in polar regions and have thereby achieved an airborne fraction close to that observed (if neglecting the role of terrestrial biota). They do, on the other hand, not consider adequately the internal consistency of their model, particularly with regard to the deep sea at low latitudes. Recently, Siegenthaler (1983) has developed a box-diffusion model also including direct transfer from the atmosphere into the deep sea through an "outcrop" covering about 10% of the ocean surface. The airborne fraction in this case becomes 61%, which value is even further reduced if the model is calibrated with transient tracer data. The crude representation of the ocean in this case makes a direct verification with the aid of oceanic data difficult.

The carbon up-take by the different reservoirs during the period 1860–1980 is also shown in Table 2. We note that the deep and bottom waters are still almost unaffected. This is a major difference as compared with the diffusion outcrop model developed by Siegenthaler (1983). There is obviously a need to provide adequate resolution in any model to permit verification of the role of the intermediate waters and the deep sea based on real ocean data. We note in this context that according to Chen and Millero (1979), excess CO_2 seems not to have penetrated much below 1000 m depth. Their data, however, do not permit a very accurate determination (cf. Chen et al., 1982). The likely up-take of CO_2 by the oceans could presumably be determined by using a model of the kind developed here, but with considerably better spatial resolution.

6.3. *Transfer of bomb-produced ^{14}C into the ocean*

Table 2 also shows the computed changes of $\Delta^{14}C$ in the oceans due to emissions of bomb-produced ^{14}C during the years 1955–74 and Fig. 17 depicts these changes as a function of time. The observed changes as compiled by Tans (1981) are also given. The computed increase is somewhat delayed during the period 1960–66 in comparison with observed changes. On the other hand the concentrations are about 40‰ too high after 1970. Both these observations are consistent with inadequate uptake by the ocean in the present model.

The observed $\Delta^{14}C$ concentration in the troposphere decreased during these 10 years from +70% to +40% (Nydal et al., 1979). If we assume that the troposphere extends up to 150 mb, this corresponds to $85 \cdot 10^{26}$ atoms. The excess ^{14}C in the stratosphere above pre-bomb conditions was $150 \cdot 10^{26}$ atoms in 1965, which value decreased to $50–60 \cdot 10^{26}$ atoms in 1974, if extrapolating the data

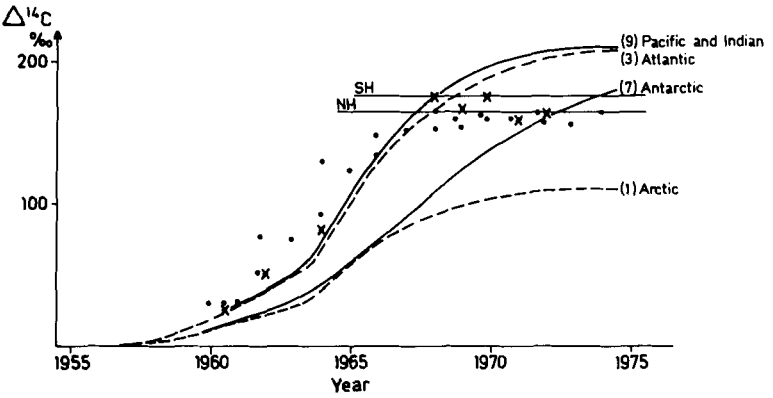

Fig. 17. Computed changes of $\Delta^{14}C$ (‰) for the four surface reservoirs due to emissions of bomb-produced ^{14}C during the period 1955–74. Observed values are shown by (.) for the Northern Hemisphere (NH) and (×) for the Southern Hemisphere (SH) and the observed quasi-constant values from 1968 to 1973 are shown by horizontal lines (data from Tans, 1981).

given by Machta (1972). Thus the total decrease in the atmosphere during this 10-year period was $180 \cdot 10^{26}$ atoms ^{14}C.

The model computations yield for the period 1965–74 a transfer to the oceans of $95 \cdot 10^{26}$ atoms ^{14}C in excess of the pre-bomb transfer. We need, however, also to consider the ^{14}C exchange between the terrestrial biota and the atmosphere. A rough estimate may be made as follows:

(i) Short-lived biota, with a total mass of about $130 \cdot 10^{15}$ g C (Bolin, 1981), has at any one time a $\Delta^{14}C$ value close to that of the atmosphere. This implies a net transfer of $30 \cdot 10^{26}$ atoms ^{14}C back to the atmosphere.

(ii) Long-lived biota has an average turnover time of about 40 years and the formation is about $15 \cdot 10^{15}$ g yr^{-1} (Bolin, 1981). Thus an amount of $150 \cdot 10^{15}$ g of wood with no ^{14}C excess has been replaced by that same amount with an average ^{14}C excess of 55%. This implies a ^{14}C transfer from the atmosphere to the terrestrial biosphere of $50 \cdot 10^{26}$ atoms ^{14}C. This is an upper limit, since some wood formed during the years 1965–74 with an excess ^{14}C presumably also has decayed.

(iii) A net carbon transfer to the atmosphere due to deforestation and oxidation of cultivated soil of $2 \cdot 10^{15}$ g C yr^{-1} corresponds to a ^{14}C transfer to the atmosphere of $10 \cdot 10^{26}$ atoms ^{14}C during a ten-year period. If on the other hand the increased CO_2 content of the atmosphere has enhanced the growth and accumulation of carbon in natural ecosystems this transfer is correspondingly less.

Table 3 summarizes the estimates above.

We find that the oceanic ^{14}C up-take as deduced with the present model can only account for 55% (95/170) of the amount necessary to balance the atmospheric ^{14}C budget. This analysis is in qualitative agreement with a similar one by Broecker et al. (1980).

Table 3. *^{14}C budget for the atmosphere during the years 1965–1974. Net transfers are given in units of 10^{26} atoms ^{14}C*

Observed decrease in the troposphere	−85
stratosphere	−95
atmosphere	−180
Computed	
decrease of ^{14}C in short-lived biota	+30
increase of ^{14}C in long-lived biota	−50
flux to atmosphere due to deforestation and net oxidation of soils	+10
transfer to the oceans to yield observed change in the atmosphere	−170
atmosphere	−180
Transfer to the oceans according to model computations	−95

We obviously need an ocean model with better spatial resolution to account properly for the oceans as a sink for excess ^{14}C emitted into the atmosphere by nuclear bomb testing. It seems likely, therefore, that the present crude model of the oceans overestimates the airborne fraction considerably. In view of the results presented by Siegenthaler (1983) a value even below 60% seems plausible.

7. Conclusions

7.1. *Methodology*

(i) The simultaneous use of a number of oceanic tracers to deduce the ocean circulation and other transfer processes has been formulated in terms of a matrix inversion method.

(ii) If a sufficiently large number of tracer distributions are known, an incompatible problem is faced which has been solved by minimizing the errors in satisfying the set of simultaneous equations deduced.

(iii) The sensitivity of the solution due to uncertainty in the data sets has been investigated and it has been shown how box configuration, spatial resolution, representativeness and accuracy of observations influence the results.

(iv) It seems advisable next to apply the method to individual oceans or parts of oceans to permit better spatial resolution and to gain further experience of its use.

(v) In later studies temperature and salinity data should be used in addition to the data for dynamically passive tracers employed in the present study.

(vi) The set of equations derived from the consideration of tracer continuity should be supplemented by dynamical constraints, e.g. quasi-geostrophic flow.

7.2. *The application of the method to a 12-box model of the ocean*

(i) In spite of crude spatial resolution, the gross features of the global ocean circulation have been deduced with a simple 12-box model of the oceans. We note particularly that

- a weak direct circulation with sinking motions in the Atlantic and rising motions in the Pacific/Indian Oceans is present at larger depths.
- tracer balance in the intermediate waters is maintained by down-welling from the Antarctic surface water, upward motions within the intermediate water reservoirs and vertical turbulent exchange with the surface water.
- strong upwelling (presumably caused by the Ekman drift due to strong eastward stress from the atmosphere) and vertical turbulent exchange are important to maintain tracer balance in the Antarctic Ocean.
- the magnitudes of organic and carbonate detritus flux in the oceans are estimated to be $4.8 \cdot 10^{15}$ g C yr^{-1} and $0.5 \cdot 10^{15}$ g C yr^{-1}, respectively.

(ii) Finally and most importantly, the use of the present ocean model to simulate the transient changes of total dissolved inorganic carbon due to fossil fuel burning and ^{14}C due to the emission of ^{14}C, reveals the inadequacy of the adopted spatial resolution to study man's impact on the global carbon cycle. It also follows that simpler models can neither be used to settle the controversy about the role of the oceans in the carbon cycle. We note particularly the need for treating the influx of CO_2 and ^{14}C into the Antarctic (and Arctic) regions properly and using better resolution in the description of the thermocline region.

8. Acknowledgement

This work has been supported by the Swedish Natural Science Research Council (NFR) under contract E-EG 223-111 and by a grant from the U.S. National Science Foundation under contract DEB-8110477.

We also wish to express our appreciation to Mrs. Siv Feusi for extensive work in typing and organizing the manuscript for publication and to Mrs. Margareta Gustafsson for drafting the figures.

9. Appendix

By ANDERS BJÖRKSTRÖM and BERRIEN MOORE

When we attempt to solve a system of r linear equations in s unknowns, such as (2.9)

$$\mathbf{A}\mathbf{x} = \mathbf{b}$$

we, in general, meet two complications. First, the matrix **A** has no inverse in the traditional sense. Algorithms for calculating the inverse of a given matrix are therefore of no direct use for us. Second, not every solution **x** can be accepted since it may not be realistic.

These two problems occur in many different applications of linear equation systems, and the mathematical literature contains methods to approach the various difficulties. In particular, the work by Lawson and Hanson (1974) has been useful to us. We nevertheless find it appropriate to devote this appendix to an almost self-contained account of how we have adapted these methods to suit the particular problem of our box model equations.

A.1. *Some concepts from linear algebra*

We denote by E^n the set of all n-tuples of real numbers (or, equivalently, the set of all $(n \times 1)$ column vectors). The concepts of *addition* of two elements of E^n and *multiplication* of an element of E^n with a real number are assumed to be known. We make the following observations.

1. By the *range* of the $r \times s$ matrix **A**, denoted $R(\mathbf{A})$, we mean the set of vectors **y** in E^r to which there exists an **x** in E^s such that $\mathbf{y} = \mathbf{Ax}$. It is easy to show that $R(\mathbf{A})$ is a subspace of E^r.

2. The *null* of **A**, denoted $N(\mathbf{A})$ is the set of vectors **x** in E^s such that $\mathbf{Ax} = 0$ (the zero vector in E^r). It is easy to show that $N(\mathbf{A})$ is a subspace of E^s.

3. For any vector **y** in E^r, the *preimage* of **y** under **A** is the set of vectors **x** in E^s such that $\mathbf{Ax} = \mathbf{y}$. The preimage is denoted $\mathbf{A}^i\mathbf{y}$. This set is in general not a subspace of E^s.

4. To any elements $\mathbf{x}^1$ and $\mathbf{x}^2$ in E^n we define a number, called the *inner product* of $\mathbf{x}^1$ and $\mathbf{x}^2$. In most cases, the inner product is defined as

$$\langle \mathbf{x}^1, \mathbf{x}^2 \rangle = \sum_{j=1}^{n} x_j^1 x_j^2$$

where x_j^i is the jth coordinate of x_i, $i = 1, 2$.

We will also meet *weighted inner products*, that is, functions of the form

$$\langle \mathbf{x}^1, \mathbf{x}^2 \rangle = \sum_{j=1}^{n} w_j x_j^1 x_j^2$$

where w_j can be arbitrary non-negative numbers. The usefulness of the inner product is that it enables us to speak of distances and projections in a linear space:

5. The *length* of a vector **x** is defined as

$$\|\mathbf{x}\| = \sqrt{\langle \mathbf{x}, \mathbf{x} \rangle}$$

and the *distance* between two vectors $\mathbf{x}_1$ and $\mathbf{x}_2$ is defined as $\|\mathbf{x}_1 - \mathbf{x}_2\|$. The concepts *close* and *remote* thus become meaningful.

6. For any subspace M of E^n, the *orthogonal complement* of M, dentoed M^c is the set of vectors **r** such that for every **m** in M

$$\langle \mathbf{r}, \mathbf{m} \rangle = 0$$

It is easy to show that M^c is a subspace.

7. Given a subspace M of E^n every **x** in E^n can be written as a sum $\mathbf{x} = \mathbf{m} + \mathbf{z}$ where **m** is in M and **z** is in M^c. This decomposition of **x** is unqiue. The function that produces **m**, given **x**, is called the (orthogonal) *projection* onto M and denoted $\mathbf{P}_M\mathbf{x}$. By analogy, $\mathbf{z} = \mathbf{P}_{M^c}\mathbf{x}$. It can easily be shown that the operators $\mathbf{P}_M$ and $\mathbf{P}_{M^c}$ are linear. It is almost immediate that $R(\mathbf{P}_M) = M$ and $N(\mathbf{P}_M) = M^c$ and that $\mathbf{P}_M\mathbf{x}$ is the closest vector in M to **x**.

A.2. *The pseudo-inverse matrix*

We can now define the pseudo-inverse for any matrix. The pseudo-inverse generalizes the concept of inverse transformations to permit us to address the two ways in which the matrix **A** may fail to have an inverse in the classical sense. Namely, if **A** is an $r \times s$ matrix mapping E^s to E^r and **y** is any vector in E^r, then **y** may not be in $R(\mathbf{A})$ or if **y** is in $R(\mathbf{A})$ then there may exist more than one **x** such that $\mathbf{Ax} = \mathbf{y}$. If neither of these difficulties applies, the pseudo-inverse gives the same result as the usual matrix inverse.

Definition. If **A** is an $r \times s$ matrix, then its *pseudo-inverse* is the linear transformation $\mathbf{A}^+$ from E^r to E^s defined for each **y** in E^r by the procedure

$$\mathbf{A}^+\mathbf{y} = \mathbf{P}_{N(\mathbf{A})^c}\mathbf{z} \qquad \text{(A.1)}$$

where **z** is any member of $\mathbf{A}^i\mathbf{P}_{R(\mathbf{A})}\mathbf{y}$. ($\mathbf{A}^i$ denotes a pre-image, see observation 3).

Informally, the definition of the pseudo-inverse $\mathbf{A}^+$ of a matrix **A** can be stated the following way: Given a vector **y**, move the smallest possible distance from **y** to reach a point $\mathbf{y}_p$ in $R(\mathbf{A})$, i.e. $\mathbf{y}_p = P_{R(\mathbf{A})}\mathbf{y}$. Let $\mathbf{A}^+\mathbf{y}$ be the **x** that satisfies $\mathbf{Ax} = \mathbf{y}_p$ or, if many such vectors **x** exist, let $\mathbf{A}^+\mathbf{y}$ be the smallest among them. We thus in a sense minimize both $\|\mathbf{Ax} - \mathbf{y}\|$ and **x**.

Almost any algorithm for determining $\mathbf{A}^+$ will be based upon singular value decomposition for $\mathbf{A}$ (Lawson and Hanson, 1974, Chapter 4). The details of this more technical aspect of linear algebra are not necessary for this discussion except to note that a by-product of the decomposition is an orthonormal set $\mathbf{z}_1, \mathbf{z}_2, \ldots, \mathbf{z}_n$ vectors that span $N(\mathbf{A})$, where n is the dimension of $N(\mathbf{A})$. By this we mean that for every vector $\mathbf{z}$ in $N(\mathbf{A})$ there is a unique set of numbers $a_1, a_2, \ldots, a_n$ such that $\mathbf{z} = a_1\mathbf{z}_1 + a_2\mathbf{z}_2 + \ldots + a_n\mathbf{z}_n$ and that $\|\mathbf{z}_j\| = 1$ for every $j = 1, \ldots, n$ and $\langle \mathbf{z}_i, \mathbf{z}_j \rangle^1{}_2{}^0$ when $i \neq j$. The set $\mathbf{z}_1, \ldots, \mathbf{z}_n$ is called an *orthonormal basis* for $N(\mathbf{A})$, and they are the singular vectors of $\mathbf{A}$ associated with singular value zero. We will make use of the vectors $\mathbf{z}_1, \ldots, \mathbf{z}_n$ in connection with "Method II" (Section A.6).

A.3. *The least square problem with linear inequality constraints (LSI)*

We now turn to the other principal complication in connection with the problem (2.9), i.e., that the solution given by

$$\mathbf{x} = \mathbf{A}^+\mathbf{b}$$

may not be physically meaningful. As noted in the text, the constraints of being physically meaningful can be expressed by the requirement that the elements of $\mathbf{x}$ satisfy a set of q linear inequalities:

$$\sum_{j=1}^{s} G_{ij} x_j \geq h_i, \quad i = 1, \ldots, q \tag{A.2}$$

for which we may use the notation

$$\mathbf{Gx} \geq \mathbf{h} \tag{A.3}$$

Recalling this, we restate the problem:

Let $\mathbf{A}$ be an $r \times s$ matrix, $\mathbf{b}$ an r-dimensional vector, $\mathbf{G}$ a $q \times s$ matrix, and $\mathbf{h}$ a q-dimensional vector. Determine the s-dimensional vector $\mathbf{x}$ such that $\|\mathbf{Ax} - \mathbf{b}\|$ is minimal, given $\mathbf{Gx} \geq \mathbf{h}$. This is known as a least squares problem with linear inequality constraints (LSI). It represents the most natural formulation of our problem (2.9). In most of the cases discussed in the text, there is a straightforward algorithm for the solution of the LSI problem. One of the tools for the solution is the so-called Least Distance Programming technique (LDP).

A.4. *The least distance programming (LDP) algorithm*

For our present purpose, we may think of the LDP algorithm as a function of two variables:

$$\mathbf{w} = \mathbf{w}(\mathbf{K}, \mathbf{k})$$

where the two arguments are an $n_r \times n_c$ matrix $\mathbf{K}$ and an n_r – dimensional vector, $\mathbf{k}$. These two define a set of n_r linear inequalities in n_c-dimensional space:

$$\mathbf{Kx} \geqslant \mathbf{k} \tag{A.4}$$

If there exists a region in the n_c-dimensional space where (A.7) is fulfilled, $\mathbf{w}$ is defined as the smallest vector in it:

$$\begin{cases} \mathbf{Kw} \geqslant \mathbf{k} \\ \|\mathbf{w}\| \text{ minimal} \end{cases} \tag{A.5}$$

We need not here consider how $\mathbf{w}$ is computed, but refer to Lawson and Hanson (1974, p. 165).

A.5. *Method I*

The most straightforward way to solve the LSI problem is to compute the r-dimensional vector

$$\mathbf{y}_0 = \mathbf{w}(\mathbf{GA}^+, \mathbf{h} - \mathbf{GA}^+\mathbf{b}) \tag{A.6}$$

and take

$$\mathbf{x}_0 = \mathbf{A}^+(\mathbf{y}_0 + \mathbf{b}) \tag{A.7}$$

The vector $\mathbf{x}_0$, in a wide class of cases, is the solution of the LSI problem. For a proof, the reader is referred to Lawson and Hanson (1974).

The method of solution may be viewed geometrically in the following way. Fig. A.1 shows the point $\mathbf{b}$ in r-dimensional space. *ABCD* is the subspace which is defined by $\mathbf{Ax}$, where $\mathbf{x}$ varies over all s-dimensional vectors. Usually the point $\mathbf{b}$ is not in the subspace (hyperplane) *ABCD*. We then rather solve for $\mathbf{Ax}_p = \mathbf{b}_p$ where $\mathbf{b}_p$ is the projection of $\mathbf{b}$ on the range of $\mathbf{A}$. This approximate solution which is obtained by minimizing $\|\mathbf{Ax} - \mathbf{b}\|$ may still yield inappropriate signs of some components of $\mathbf{x}$ (e.g. negative turbulent exchange coefficients). There is, however, one part of the subspace *ABCD* (indicated by shading) which corresponds to those values of $\mathbf{x}$, for which all components satisfy the additional conditions $\mathbf{Gx} \geqslant \mathbf{h}$. The point $\mathbf{b}_d$ which is closest to $\mathbf{b}$ corresponds to the solution $\mathbf{x}_d$ where $\mathbf{Ax}_d = \mathbf{b}_d$ and is obtained by an additional minimizing procedure.

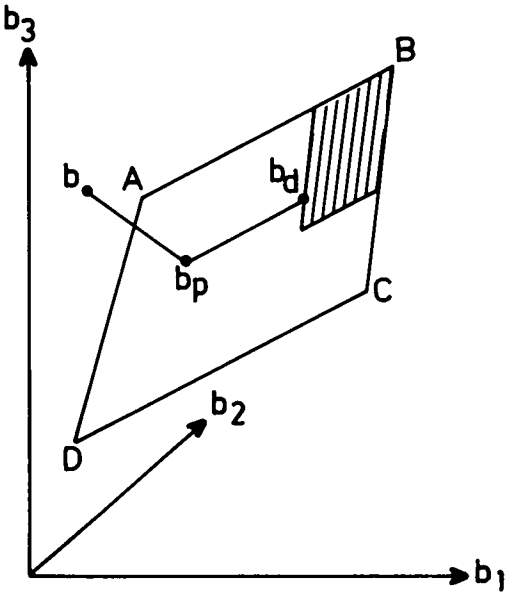

Fig. A.1. Example of position of the point **b** in an r-dimensional space. The points $\mathbf{b}_p$ and $\mathbf{b}_d$ are in the plane $ABCD$; the vector from **b** to $\mathbf{b}_p$ is orthogonal to this plane.

It is important to note, however, that the method requires that $N(\mathbf{A})$ consist of the zero vector only. In some of the applications, we deal with situations where the number of equations is considerably smaller than the number of unknowns. At present, we treat these cases by a different method.

A.6. *Method II*

The case when the dimension of $N(\mathbf{A})$ is greater than zero is treated as follows. We start with $\mathbf{x}_0 = \mathbf{A}^+\mathbf{b}$ and adjust $\mathbf{x}_0$ by using a vector from $N(\mathbf{A})$ such that the resulting vector **x** satisfies $\mathbf{Gx} \geq \mathbf{h}$ and $\|\mathbf{Ax} - \mathbf{b}\| = \|\mathbf{Ax}_0 - \mathbf{b}\| = 0$. This approach tends to fail when $N(\mathbf{A})$ is small; however, the requirement $\|\mathbf{Ax} - \mathbf{b}\| = 0$ is then perhaps too strong.

We shall demonstrate this approach to the LSI problem with the following example. Let the number of rows in **G** be a number q which is smaller than the number of dimensions of **x**, s. Define the element G_{ij} to be

$$G_{ij} = \begin{cases} 1 & \text{if } j = i + (s - q) \\ 0 & \text{otherwise} \end{cases}$$

and let the vector **h** be the zero vector in E^q. In other words, **G** consists of a $q \times (s - q)$ zero matrix followed to its right by a $q \times q$ identity matrix. The inequalities now formulated will require the last q coordinates of the vector **x** to be non-negative.

The strategy is to determine a vector $\mathbf{z}_0$ in $N(\mathbf{A})$ such that $\|\mathbf{z}_0\|$ is minimal and the last q coordinates of $\mathbf{x}_0 + \mathbf{z}_0$ are non-negative. In other words, the problem becomes one of finding real numbers $a_1, a_2, \ldots, a_n$ such that

$$a_1\mathbf{z}_1 + \ldots + a_n\mathbf{z}_n \tag{A.8}$$

is the desired vector $\mathbf{z}_0$, where $\mathbf{z}_1, \ldots, \mathbf{z}_n$ is an orthonormal basis of $N(\mathbf{A})$. The conditions

$$(\mathbf{x}_0 + \mathbf{z}_0)_j \geqslant 0 \quad \text{for } j = s - q + 1, \ldots, s \tag{A.9}$$

can be restated as

$$\sum_{i=1}^{n} a_i(\mathbf{z}_i)_j \geqslant -(\mathbf{x}_0)_j \quad \text{for } j = s - q + 1, \ldots, s \tag{A.10}$$

The condition of minimal $\|\mathbf{z}_0\|$ is equivalent to the condition of minimal $\sum_{i=1}^{n} |a_i|^2$. This follows because

$$\|\mathbf{z}_0\|^2 = \left\| \sum_{i=1}^{n} a_i\mathbf{z}_i \right\|^2 = \sum_{i=1}^{n} a_i^2 \|\mathbf{z}_i\|^2 = \sum_{i=1}^{n} a_i^2 \tag{A.11}$$

where the last two equalities are consequences of the orthonormality of the vectors $\mathbf{z}_i$.

The relations (A.10) can be written in matrix form if we define a $q \times n$ matrix **K** such that

$$\mathbf{K} = \begin{bmatrix} (\mathbf{z}_1)_{s-q+1} & (\mathbf{z}_2)_{s-q+1} & (\mathbf{z}_n)_{s-q+1} \\ (\mathbf{z}_1)_{s-q+2} & \cdots & \vdots \\ \vdots & & \vdots \\ (\mathbf{z}_1)_s & \cdots & (\mathbf{z}_n)_s \end{bmatrix}$$

and a q-dimensional vector k such that

$$(\mathbf{k})_j = -(\mathbf{x}_0)_{s-q+j} \quad j = 1, \ldots, q$$

If we now use the LDP algorithm to compute an n-dimensional vector **a**:

$$\mathbf{a} = \mathbf{w}(\mathbf{K}, \mathbf{k})$$

we will obtain as result a set of numbers a_i (if one exists) that fulfills

$$\mathbf{Ka} \geqslant \mathbf{k}, \quad \|\mathbf{a}\| \text{ minimal}$$

This is equivalent to condition (A.10) and the condition of minimal $\|\mathbf{z}_0\|$. We can thus obtain $\mathbf{z}_0$ from (A.8) by using the numbers a_i.

REFERENCES

Almgren, T., Dyrssen, D. and Strandberg, M. 1975. Determination of pH on the moles per kg seawater scale (Mw). *Deep-Sea Res. 22*, 635–646.

Anderson, L. and Dyrssen, D. 1981. Chemical constituents of the Arctic Ocean in the Svalbard area. *Oceanologica Acta 4*, 3, 305–311.

Bacastow, R. and Björkström, A. 1981. Comparison of ocean models for the carbon cycle. In *Carbon cycle modelling* (ed. B. Bolin). SCOPE 16, 29–79. Chichester: John Wiley & Sons.

Bacastow, R. and Keeling, C. D. 1981. Atmospheric carbon dioxide concentration and the observed airborne fraction. In *Carbon cycle modelling* (ed. B. Bolin). SCOPE 16, 103–112. Chichester: John Wiley & Sons.

Bolin, B. 1981. Steady state and response characteristics of a simple model of the carbon cycle. In *Carbon cycle modelling* (ed. B. Bolin). SCOPE 16, 315–331. Chichester: John Wiley & Sons.

Bolin, B. 1983. Changing global biogeochemistry. In *Oceanography, the present and future* (ed. P. Brewer), 305–326. New York: Springer Verlag.

Bolin, B., Degens, E. T., Duvigneaud, P. and Kempe, S. 1979. The global biogeochemical carbon cycle. In *The global carbon cycle* (eds. B. Bolin, E. T. Degens and S. Kempe). SCOPE 13, 1–56. Chichester: John Wiley & Sons.

Brewer, P. G. and Goldman, S. C. 1976. Alkalinity changes generated by phytoplankton growth. *Limnol. and Oceanogr. 21*, 108–117.

Broecker, W. S., Gerard, R., Ewing, M. and Heezen, B. C. 1960. Natural radiocarbon in the Atlantic Ocean. *J. Geoph. Res. 65*, 2903–2931.

Broecker, W. S. and Peng, T.-H. 1974. Gas exchange rates between air and sea. *Tellus 26*, 21–35.

Broecker, W. S., Peng, T.-H. and Engh, R. 1980. Modelling the carbon system. *Radiocarbon 22*, 565–598.

Chen, C.-T. 1978. Deposition of calcium carbonate and organic carbon in the deep ocean. *Science 201*, 735–736.

Chen, C.-T. and Pytkowicz, R. M. 1979. On the total CO_2-titration alkalinity-oxygen system in the Pacific Ocean. *Nature 281*, 362–365.

Chen, C. T. and Millero. F. J. 1979. Gradual increase of oceanic carbon dioxide. *Nature 277*, 205–206.

Chen. C.-T., Millero, F. J. and Pytkowicz, R. M. 1982. Comment on calculating the oceanic CO_2 increase: A need for caution by A. M. Shiller. *J. Geoph. Res. 87, C3*, 2083–2085.

Defant, A. 1961. *Physical oceanography*. Oxford: Pergamon Press.

Fiadeiro, M. E. 1983. Physical-chemical processes in the open sea. In *The major biogeochemical cycles and their interactions* (eds. B. Bolin and R. B. Cook). SCOPE 21, 463–478. Chichester: John Wiley & Sons.

Fine, R. A., Reid, J. L. and Östlund, H. G. 1981. Circulation of tritium in the Pacific Ocean. *J. Phys. Oceanog. 11*, 3–14.

Gordon, A. L. 1971. Oceanography of Antarctic waters. *Antarctic Res. Series 15*, 169–203. Am. Geoph. Union. National Academy of Sciences, Washington, D.C.

Hanson, I. 1973. A new set of acidity constants for carbon acid and boric acid in sea water. *Deep-Sea Res. 20*, 461–478.

Keeling, C. D. 1973. The carbon dioxide cycle: Reservoir models to depict the exchange of atmospheric carbon dioxide with the oceans and land plants. In *Chemistry of the lower atmosphere* (ed. S. I. Rasool). New York: Plenum Press, 251–329.

Keeling, C. D. and Bolin, B. 1967. The simultaneous use of chemical tracers in oceanic studies. I. General theory of reservoir models. *Tellus 19*, 566–581.

Keeling, C. D. and Bolin, B. 1968. The simultaneous use of chemical tracers in oceanic studies. II. A three-reservoir model of the North and South Pacific oceans. *Tellus 20*, 17–54.

Kuo, H. H. and Veronis, G. 1970. Distribution of tracers in the deep oceans of the world. *Deep-Sea Res. 17*, 29–46.

Lawson, C. L. and Hanson, R. J. 1974. *Solving least squares problems*. Englewood Cliffs, N.J.: Prentice-Hall Inc.

Liss, P. S. 1983. The exchange of biogeochemically important gases across the air-sea interface. In *The major biogeochemical cycles and their interactions* (eds. B. Bolin and R. B. Cook). SCOPE 21, 411–426. Chichester: John Wiley & Sons.

Machta, L. 1972. The role of the oceans and the biosphere in the CO_2 cycle. In *Changing chemistry of the oceans* (ed. D. Dyrssen). Nobel Symposium No 20. Stockholm: Almqvist & Wiksell.

Mehrbach, C., Culberson, C. H., Hawley, J. E. and Pytkowicz, R. M. 1973. Measurements of the apparent dissociation constants of carbonic acid in sea water at atmospheric pressure. *Limnol. Oceanogr. 18*, 897–907.

Moore, B., Boone, R. D., Hobbie, J. E., Houghton, R. A., Melillo, J. M., Peterson, B. J., Shaver, G. R., Vörösmarty, C. J. and Woodwell, G. M. 1981. A simple model for analysis of the role of terrestrial ecosystems in the global carbon budget. In *Carbon cycle modelling* (ed. B. Bolin). SCOPE 16, 365–386. Chichester: John Wiley & Sons.

Munk, W. 1966. Abyssal recipies. *Deep-Sea Res. 13*, 707–730.

Nydal, R., Lövseth, K. and Gulliksen, S. 1979. A survey of radiocarbon variation in nature since the Test Ban Treaty. In *Proc. 9th Int. Conf. Radiocarbon Dating*, California 1976.

Oeschger, H., Siegenthaler, U., Schotterer, U. and Gugelmann, A. 1975. A box diffusion model to study

the carbon dioxide exchange in nature. *Tellus 27*, 168–192.

Peng, T.-H., Broecker, W. S., Mathieu, G. G. and Li, Y.-H. 1979. Radon evasion rates in the Atlantic and Pacific oceans as determined during the GEOSECS program. *J. Geophys. Res. 85*, 2471–2486.

Redfield, A. C. 1958. The biological control of chemical factors in the environment. *Am. Sci. 46*, 206–226.

Rotty, R. 1981. Data for global CO_2 production from fossil fuels and cement. In *Carbon cycle modelling* (ed. B. Bolin). SCOPE 16, 121–124. Chichester: John Wiley & Sons.

Shilov, G. S. 1961. *An introduction to the theory of linear spaces*. Englewood Cliffs, N.J.: Prentice-Hall Inc.

Siegenthaler, U. 1983. Uptake of excess CO_2 by an outcrop-diffusion model of the ocean. *J. Geoph. Res.* (in press).

Stuiver, M. 1980. ^{14}C distribution in the Atlantic Ocean. *J. Geoph. Res. 85*, 2711–2717.

Stuiver, M., Östlund, H. G. and McConnaughey, T. A. 1981. GEOSECS Atlantic and Pacific ^{14}C distributions. In *Carbon cycle modelling* (ed. B. Bolin). SCOPE 16, 201–222. Chichester: John Wiley & Sons.

Stuiver, M. and Quay, P. D. 1981. Atmospheric ^{14}C changes resulting from fossil fuel CO_2 release and cosmic ray flux variability. *Earth and Planetary Science Letters 53*, 349–362.

Takahashi, T. and Broecker, W. S. 1977. Mechanisms for calcite dissolution on the sea floor. In *The fate of fossil fuel CO_2 in the oceans* (eds. N. Andersen and A. Malakoff). New York: Plenum Press, 455–477.

Takahashi, T., Broecker, W. S. and Bainbridge, A. E. 1981. Supplement to the alkalinity and total carbon dioxide concentration in the world oceans. In *Carbon cycle modelling* (ed. B. Bolin). SCOPE 16, 159–199. Chichester: John Wiley & Sons.

Tans, P. 1981. A compilation of bomb ^{14}C data for use in global carbon model calculations. In *Carbon cycle modelling* (ed. B. Bolin). SCOPE 16, 131–157. Chichester: John Wiley & Sons.

Viecelli, J. A., Ellsaesser, H. W. and Burt, J. E. 1981. A carbon cycle model with latitude dependance. *Climatic Change 3*, 281–302.

Weiss, R. F. 1970. The solubility of nitrogen oxygen and argon in water and seawater. *Deep-Sea Res. 17*, 721–735.

Weiss, R. F. 1974. Carbon dioxide in water and seawater: The solubility of a non-ideal gas. *Marine Chemistry 2*, 203–215.

Wunsch, C. and Minster, J.-F. 1982. Methods for box models and ocean circulation tracers: Mathematical programing and non-linear inverse theory. *J. Geoph. Res. 87*, 5647–5662.

Wyrtki, K. 1962. The oxygen minima in relation to ocean circulation. *Deep-Sea Res. 9*, 11–23.